Anterior-posterior polarity signals differentially regulate regeneration-competence of the tapeworm *Hymenolepis diminuta*.

Elise McCollough Nanista[1], Landon Elizabeth Poythress[1], Isabell Reese Skipper[1], Trevor Haskins[1], Marieher Felix Cora[2] and Tania Rozario[1]*

[1]University of Georgia, Athens, GA, USA

[2]University of Puerto Rico-Cayey, PR, USA

Running title: Tapeworm regeneration-competence

* corresponding author

tania.rozario@uga.edu

500 D.W. Brooks Dr., Athens, GA 30602, USA

ORCIDS:

EMN: 0009-0002-3844-876X

LEP: 0009-0007-5836-5714

IRS: 0009-0009-1869-7292

TH: 0009-0007-1528-3807

MFC: 0009-0004-9971-0826

TR: 0000-0002-9971-5211

Keywords: regeneration, tapeworm, planaria, flatworm, Wnt signaling

Abstract

Competence to regenerate lost tissues varies widely across species. The rat tapeworm, *Hymenolepis diminuta*, undergoes continual cycles of shedding and regenerating thousands of reproductive segments to propagate the species. Despite its prowess, *H. diminuta* can only regenerate posteriorly from a singular tissue: the neck or germinative region (GR). What cells and signaling pathways restrict regeneration competence to the GR? In this study, we show that the head regulates regeneration-competence by promoting maintenance of the GR and inhibiting proglottid formation in a distance-dependent manner. Anterior-posterior (A-P) patterning within the GR provide local signals that mediate these head-dependent responses. *βcat1* is necessary for stem cell maintenance, proliferation and proglottidization. On the other hand, *sfrp* is necessary for maintaining the GR at its proper length. Our study demonstrates that the head organizes a balance of pro- and anti-regeneration signals that must be integrated together and therefore control competence to regenerate.

Summary statement

We uncover how the tapeworm head organizes pro- and anti-regeneration signals that control competence to regenerate at prolific rates.

43 **Introduction**

44

45 Regeneration occurs over a wide range of biological scales from regeneration of axons at the
46 cellular scale to whole body regeneration in planarians and hydra (Bely and Nyberg, 2010).
47 Tapeworms represent a fascinating case study in the field of regeneration. They descend from a
48 monophyletic clade (Neodermata) exclusively populated by parasites within the Playhelminthes
49 phylum (Laumer et al., 2015). As a sister group to planarians, it is tempting to assume that shared
50 regenerative abilities have enabled tapeworms to achieve their monstrous growth potential and
51 reproductive prowess. In the normal life cycle of many adult tapeworms, large pieces of their body
52 are shed to disperse the developing embryos for consumption by an intermediate host.
53 Simultaneously, the adult tapeworm continues to replenish the lost tissue in the intestine. Studies
54 with the rat tapeworm, *Hymenolepis diminuta*, demonstrated that serially transplanting anterior
55 pieces of tapeworms into new host intestines could greatly extend the lifespan of this parasite
56 (Goodchild, 1958; Read, 1967). *H. diminuta* can regenerate all lost reproductive segments
57 (proglottids) and may not inherently need to age and die. However, regeneration only occurs from
58 one anatomical structure: the neck or germinative region (GR) (Rozario et al., 2019). *H. diminuta*
59 regeneration is dependent on a large and heterogeneous population of adult stem cells that are
60 distributed throughout the body and do not preferentially reside in the GR (Rozario et al., 2019).
61 By transplanting cells from regeneration-competent and regeneration-incompetent regions into
62 lethally irradiated tapeworm GRs, we previously demonstrated that proglottid regeneration is
63 independent of stem cell source (Rozario et al., 2019), suggesting that signals within the GR play
64 important roles in regulating tapeworm regeneration.

65

66 A plethora of signals likely operate in the GR and control stem cell proliferation, survival,
67 differentiation, as well as proglottidization and competence to regenerate. What these signals are
68 and how they operate is largely unknown. Here we show that regeneration competence is tightly
69 linked to signals from the head. The head plays seemingly contradictory roles as it is necessary to
70 maintain the GR but negatively regulates proliferation and proglottid regeneration. We find two
71 genes typically associated with Wnt signaling, *sfrp and βcatenin1*, as critical mediators of each
72 head-dependent phenotype. Our study demonstrates that for successful proglottid regeneration to
73 occur, a balance of pro- and anti-regeneration signals must be overcome to enable GR regeneration

74 and then initiation of proglottids. *H. diminuta* provides a fascinating example of how extrinsic
75 signals can promote or restrict the ability to regenerate.

76 **Results**

77 ***H. diminuta* is competent to regenerate the GR.**

78 The basic adult body plan of *H. diminuta* includes a head (scolex), an unsegmented GR and a
79 strobilated body made of metameric proglottids (Fig. 1A). *H. diminuta* cannot regenerate its
80 anterior or head but can regenerate proglottids from the GR when amputated outside of the GR
81 (Rozario et al., 2019). The GR is the only regeneration-competent tissue, but it is unclear if the
82 GR itself can regenerate. Nuclei staining with DAPI enables a quick and easy way to observe and
83 measure the GR, which is defined as the region between the base of the head and the first
84 proglottid. When tapeworms are continuously grown in vitro, the GR length is typically 1 mm
85 (Rozario et al., 2019). After acclimating worms to in vitro culture conditions for 3 days, we
86 amputated within the GR (0.5 mm) vs. outside the GR (2 mm) and grew the anterior fragments for
87 15 days. In both cases, proglottids were regenerated (Fig. 1A). Regenerates that were amputated
88 within the GR, successfully formed 1 mm long GRs 15 days post amputation (dpa) comparable to
89 regenerates that were amputated outside of the GR (Fig. 1B). The 0.5 mm fragments first
90 regenerated GRs within 2-4 days before new proglottids were added (Fig. 1C). Once proglottids
91 were formed, the rate of proglottid regeneration was comparable between 0.5 mm and 2 mm
92 fragments, at 14-15 proglottids per day (Fig. 1C). Growth curves for both regenerates were also
93 comparable and non-linear since individual proglottids increase in length as they mature (Rozario
94 et al., 2019). Thus, when amputated within the GR, *H. diminuta* is capable of regenerating the
95 posterior GR and subsequently proglottids.

96

97 The GR is patterned by differentially expressed genes along the anterior-posterior (A-P) axis
98 (Rozario et al., 2019). If *H. diminuta* can regenerate its GR, then A-P polarized patterns should be
99 restored following amputation. We performed whole mount in situ hybridization (WISH) for three
100 posterior-enriched transcripts: *βcatenin1* (*βcat1*), *frizzled5/8* (*fzd5/8*), and *tumor necrosis factor*
101 *receptor-16* (*tnfr16*) and one anterior-enriched transcript: *secreted frizzled related protein* (*sfrp*)
102 (Fig. 1D; uncut). At 0 dpa, all markers were reduced or lost but normal A-P polarized patterns in
103 successful regenerates were restored by at least 10 dpa demonstrating normal GR patterning (Fig.
104 1D). These data indicate that *H. diminuta* can successfully regenerate its GR and reestablish AP
105 patterning within 10 days.

106

107 **GR regeneration fails after serial amputation.**

108 Regeneration of proglottids is a stem cell-driven process and can occur after multiple rounds of
109 serial amputation (Goodchild, 1958; Read, 1967; Rozario et al., 2019). Is GR regeneration
110 similarly robust? We amputated worms within the GR and allowed them to regenerate for 18 days
111 before re-amputating within the GR (Fig. 2A). Subsets of each group were fixed and analyzed to
112 capture the variation and reproducibility of the amputations performed. Amputations were targeted
113 at the half-way point or ~0.5 mm in worms that were briefly immobilized in cold media. We find
114 that tissues extend slightly after heat-killing and fixation resulting in slightly longer 0 dpa
115 fragments: 0.63±0.07 mm and 0.61±0.16 mm after each amputation (Fig. 2B). The percentage of
116 GR length retained calculated over the mean GR length of uncut worms was close to the target
117 range of 50% and was not statistically significant between the two amputations (48±9% after cut
118 1 and 56±11% after cut 2) (Fig. 2C). Despite making comparable cuts at each timepoint, marked
119 differences in regeneration were observed after the second amputation within the GR (Fig. 2D-F).
120 Successful regenerates were almost always produced after cut 1 but ranged wildly between 10-
121 100% regeneration after cut 2 (Fig. 2E). When worms did regenerate after cut 2, they were
122 significantly shorter (Fig. 2D) and produced fewer proglottids (Fig. 2F). The additional challenge
123 of serial amputation revealed that GR regeneration does fail under certain conditions.

124

125 **Signals from the head regulate proglottid regeneration and maintenance of the GR.**

126 When amputated within the GR, the wound site was closer to the head. Could the head be exerting
127 a negative effect on regeneration? Following head amputation, regenerates exhibited increased
128 growth and proglottid regeneration (Fig. 3A) indicating that signals from the head do inhibit
129 growth. Using thymidine analog F-*ara*-EdU incorporation to quantify the density of proliferating
130 cells in the GR, we found that head amputation resulted in increased proliferation, which can
131 explain the increased growth (Fig. 3B). In uncut worms, proliferation density in the GR increases
132 with distance from the head (Fig. 3C) further supporting our conclusion that the head provides
133 anti-proliferation signals. Upon head amputation and in vitro culture for 3 days, the increasing
134 proliferation density along the GR A-P axis was no longer significant (Fig. 3D). However, the
135 curves did not fully flatten and the pattern of decreased proliferation toward the most anterior was
136 still detectable. This suggests that while signals from the head do regulate proliferation in the GR,
137 the effects are mediated by factors resident within the GR as well.

138

139 Many regenerating animals respond by increasing proliferation at the wound site. Is this true in *H.*
140 *diminuta*? Following amputation in the GR, we quantified proliferation at both anterior- and
141 posterior-facing wounds and found increased proliferation (Fig. S1). However, the local increase
142 in proliferation was equivalent regardless of head presence (Fig. S1) indicating that amputation
143 itself does not explain the increased proliferation in -head regenerates. This implies that the head
144 does indeed negatively regulate proliferation.

145

146 In addition to proliferation within the GR, maintenance of GR tissue must also be preserved as
147 regeneration cannot occur without it. Previous results have shown that GR maintenance depends
148 on the head; after head amputation, the GR is eventually lost, the regenerates become fully
149 proglottidized and cannot continue adding proglottids (Rozario et al., 2019). To further
150 characterize how the head affects proglottid regeneration and GR maintenance, four amputation
151 schemes were compared: + head, ½ head, -head, and -0.5 mm anterior (Fig. 4A). Of these four
152 schemes, making transverse cuts through the head was the most challenging. A sampling of ½
153 head fragments were fixed immediately and stained with anti-SYNAPSIN antibodies to visualize
154 the nervous system. Though the amount of head tissue removed did vary, the brain was always
155 retained (Fig. S2A: yellow arrowheads). After making the four different amputations at the anterior
156 region, we tested how the four fragment types would regenerate following serial amputation. All
157 worms were amputated posteriorly to obtain 2 mm fragments that were grown in vitro for 14 days,
158 then re-amputated for 3 more cycles (Fig. 4A). The posteriors of regenerates were fixed and
159 analyzed to determine the number of proglottids regenerated after every cycle. As previously
160 reported (Rozario et al., 2019), tapeworms regenerated after serial amputation when the head was
161 present (Fig. 4B). The ½ head regenerates consistently displayed increased proglottid regeneration
162 compared to +head regenerates (Fig. 4B). Both +head and ½ head regenerates maintained their
163 GRs throughout 2 months of in vitro culture. When the head was amputated completely (-head),
164 proglottid regeneration eventually ceased though some regenerates still had GRs after the 4th
165 amputation (Fig. 4B). However, the GR lengths in -head regenerates that were not fully
166 proglottidized were significantly shorter (Fig. S2B) indicating that complete proglottidization was
167 imminent. Previously, we observed rapid loss of the GR after head amputation, but anterior GR
168 tissue was also removed in those experiments (Rozario et al., 2019). Cognizant of regional

169 differences along the A-P axis of the GR, we were careful to make minimal head amputations that
170 retained as much anterior GR as possible in this study. We find that the GR persists for much
171 longer than previously reported but does eventually recede. On the other hand, fragments in which
172 both the head and anterior GR were removed (-0.5 mm) became fully proglottidized by the second
173 amputation or earlier (Fig. 4B). In sum, GRs were maintained if the brain region was retained but
174 GRs were lost when more and more anterior tissue was removed (Fig. 4C).
175
176 The number of proglottids regenerated was also dependent on amputations at the head though our
177 analysis was complicated by GR loss in -head and -0.5mm fragments. After the first amputation,
178 a clear dose-dependent response was detected; when more head tissue was retained, the number of
179 proglottids decreased (Fig. S2C). This trend was maintained after serial rounds of amputation when
180 comparing +head and ½ head regenerates where GRs were not lost (Fig. S2D). After the 4th round
181 of amputation, the remaining head area plotted against number of proglottids for +head and ½ head
182 regenerates revealed a negative correlation between head tissue abundance and proglottidization
183 (Fig. 4D). We also measured the effect of head tissue abundance on proliferation within the GR
184 using F-*ara*-EdU. A general trend of increasing proliferation with decreasing head and anterior
185 tissue emerged though differences between +head and ½ head were not statistically significant
186 (Fig. 4E-F). Taken together, the head effects on maintaining the GR and regulating proliferation
187 can be separated. Signals from the brain region are necessary to maintain the GR whereas
188 proliferation and proglottidization are regulated by head-dependent signals in a dose-dependent
189 manner.
190
191 ***βcatenin1* is necessary for proglottid regeneration and stem cell maintenance.**
192 What is the molecular basis for the head-dependent effects on tapeworm regeneration? The Wnt
193 signaling pathway has been implicated in A-P polarity across many systems (Petersen and
194 Reddien, 2009) and plays roles in regulating cell proliferation, survival, and differentiation (Nusse
195 and Clevers, 2017). Multiple members of the Wnt signaling pathway were found to be either
196 anterior-enriched or posterior-enriched after RNA sequencing along the A-P axis of the GR
197 (Rozario et al., 2019). As βcatenin protein is a key downstream effector of Wnt signaling, we
198 decided to examine its function further. *H. diminuta* has three *βcatenin* paralogs as do other
199 parasitic flatworms (Montagne et al., 2019). BLASTp comparisons of putative *H. diminuta*

200 *βcatenin* paralogs with published sequences for other flatworms (*Schmidtea medditerranea*,
201 *Schistosoma mansoni and Ecchinococcus multilocularis*) demonstrated that *Hdim-βcat1*
202 (WMSIL1_LOCUS14475) is the rat tapeworm ortholog of *βcat1* (Table S1). *Hdim-βcat1* retains
203 expected conserved domains including multiple armadillo repeats and the DSGxxSxxx[S/T]xxxS
204 motif for CKI/GSK-phosphorylation necessary for targeting by the destruction complex
205 (Montagne et al., 2019; Valenta et al., 2012) (Fig. S3A). Capacity to bind α-catenin cannot be
206 ruled in or out at present (Fig. S3B; discussed further below). Thus *Hdim-βcat1* likely mediates
207 Wnt signaling and may also function in cell adhesion.
208
209 Where is *Hdim-βcat1* (hereafter *βcat1*) expressed in *H. diminuta*? In 6-day-old adults, *βcat1*
210 expression is largely absent in the head and anterior GR but progressively increases toward the
211 posterior GR (Fig. 5A). *βcat1* is also expressed throughout the body, in transverse stripes at
212 proglottid boundaries and within a subset of accessory reproductive structures (Fig. S4). The broad
213 expression pattern throughout the worm indicates that *βcat1* is expressed in many tissues and is
214 not restricted to a particular cell type. The posterior-biased pattern of *βcat1* expression was
215 restored after successful GR regeneration (Fig. 1D) leading us to wonder if *βcat1* is necessary for
216 proliferation and proglottidization from the GR. We performed RNAi by injecting double-stranded
217 RNA (dsRNA) targeting *βcat1* throughout the GR. 2 mm anterior fragments were amputated and
218 grown in vitro to assay regenerative ability. A dramatic growth defect was captured just 7 dpa/10
219 days post injection (dpi) (Fig. 5B). Decreased growth was evident by 3 dpa and this RNAi
220 treatment was ultimately lethal. The proglottids formed were extremely small and impossible to
221 quantify but there was a marked decrease in worm lengths following *βcat1* RNAi (Fig. 5C). RNAi
222 of *βcat1* reduced transcript levels to 8.7±2.0% (Fig. 5D). As *βcat1*-dependent Wnt signaling is
223 mediated through degradation of βCAT1 protein by the destruction complex, we investigated
224 expression of a key destruction complex component: *axin1*. Previous work has demonstrated that
225 tapeworm *E. multilocularis,* AXIN proteins directly interact with Emul-βCAT1 and
226 overexpression of Emul-AXIN1 results in degradation of Emul-βCAT1 (Montagne et al., 2019).
227 We find that after *βcat1* RNAi, *axin1* expression is markedly reduced to 18.8±11.1% of normal
228 levels (Fig. 5D). This suggests that canonical Wnt signaling is inhibited following *βcat1* RNAi
229 though other roles for *βcat1* cannot be ruled out.

230

231 The strong decrease in growth after *βcat1* RNAi suggests that the cycling stem cell population in
232 the GR is likely dependent on *βcat1*. We measured proliferation in the GR and detected a dramatic
233 decrease in dividing cells compared to controls (Fig. 5E). This suggests that the stem cell
234 population likely cannot be maintained in the absence of *βcat1*. To visualize the stem cell
235 population, we performed WISH for two known stem cell markers in *H. diminuta*:
236 *minichromosome maintenance complex component-2* (*mcm2*) and *laminB receptor* (*lbr*) (Rozario
237 et al., 2019). Both stem cell markers showed decreased expression indicating that *βcat1* is required
238 to maintain stem cells in the GR (Fig. 5F).
239

240 **GR maintenance requires *sfrp*.**

241 Our analyses so far suggest that signals from the head set up gene expression patterns within the
242 GR with posteriorly enriched *βcat1* playing indispensable roles in maintaining stem cells.
243 However, it is unclear if *βcat1* regulates stem cell maintenance through Wnt signaling, cell
244 adhesion or both. If Wnt signaling is necessary, the head may segregate Wnt inhibitors toward the
245 anterior. Previously, RNA sequencing of A-P polarized transcripts in the GR found that *sfrp* was
246 anterior-enriched (Rozario et al., 2019). Like other tapeworms, *H. diminuta* has one true *sfrp*
247 family member and a second highly divergent member, *sfrp-like*, which was not investigated
248 further in this study. Interpro (Blum et al., 2020) predicts that Hdim-SFRP retains both frizzled
249 and netrin domains albeit with some variation (Fig. S5; discussed further below). Since SFRP can
250 inhibit Wnt signaling (Leyns et al., 1997; Rattner et al., 1997; Wang et al., 1997), we decided to
251 pursue its potential role in regeneration.
252

253 By WISH, *sfrp* expression is strikingly anterior-enriched. We detected *sfrp* expression sparsely
254 within the head and strongly throughout the GR with expression tapering off posteriorly (Fig. 6A).
255 In adult tapeworms, *sfrp* expression is largely absent from the strobilated body except at the lateral
256 ends of proglottids (Fig. S4). Perhaps knocking down *sfrp* would result in the opposite phenotypes
257 observed from *βcat* RNAi and would phenocopy head amputation. We injected dsRNA into the
258 head, amputated 2 mm anterior fragments, reinjected dsRNA into the head and collected worms at
259 10-12 dpa (Fig. 6B). Contrary to our expectations, a modest decrease in worm lengths and
260 proglottid regeneration were observed (Fig. 6C-D). Strikingly, we discovered that the GRs were

261 significantly shortened following *sfrp* RNAi (Fig. 6E-F). This is the first time GR length has been
262 affected by RNAi of any target gene. Injecting dsRNA into the head does not preclude diffusion
263 into the GR but the knockdown is likely to be anteriorly biased. If so, we may inadvertently miss
264 other potential roles for *sfrp* toward the posterior GR. We injected dsRNA throughout the GR and
265 observed the same phenotypes (Fig. S6A-D). Both injection schemes resulted in similar *sfrp*
266 knockdown efficacy (Fig. S6E). While the levels of knockdown did vary substantially, GR length
267 reduction was consistently observed.
268
269 Our results indicate that *sfrp* is necessary for proper GR maintenance but is unlikely to be involved
270 in head-dependent inhibition of proliferation or proglottidization. Instead, *sfrp* likely mediates
271 head-dependent GR maintenance. Accordingly, we observed decreased *sfrp* expression just 3 days
272 after head amputation (Fig. 6G). This correlation supports the conclusion that the failure to
273 maintain the GR after head amputation is mediated through anterior-enriched *sfrp* expression.
274
275 Decreased proglottid regeneration after *sfrp* RNAi does not support the hypothesis that *sfrp*
276 functions as a Wnt inhibitor. Proliferation within the GR was not significantly changed after *sfrp*
277 RNAi (Fig. S5D). However, the shortening of the GR would bring the posterior boundary of the
278 GR closer to the head. Thus, *sfrp* RNAi may indirectly exacerbate the anti-proglottidization and
279 anti-proliferation effects from the head.
280
281 **Amputation distance from the head determines whether pro- or anti-regeneration signals**
282 **dominate.**
283 The mechanisms that govern the two head-dependent effects on regeneration have begun to
284 emerge. The presence of the head is necessary for *sfrp* expression and GR maintenance. However,
285 the presence of the head also inhibits proliferation and proglottidization, which are dependent on
286 *βcat1*. Perhaps when the posterior wound is too close to the head, the growth inhibitory effect of
287 the head dominates, and GR regeneration fails. This suggests that regeneration would fail more
288 when the posterior cut is made at decreasing distance from the head. To test this, worms were
289 allowed to regenerate after 0.5 mm amputation within the GR and then cut a second time at 4
290 different distances from the head. All samples were cut at ~1mm and then subsets were
291 progressively shaved closer and closer toward the head (Fig. 7A; cuts A-D). Subsets of fragments

292 were fixed at 0 dpa and we verified that cut A-D progressively retained 87±5%, 64±7%, 47±9%,
293 and 22±4% of the GR (Fig. 7B). As expected, GR and proglottid regeneration plummeted at cut B
294 or C over three independent experiments (Fig. 7C). Surprisingly, the smallest fragments (cut D)
295 regenerated equivalently to the longest fragments (cut A) (Fig. 7C-D and Fig. S7). Fragments from
296 cut A and D achieved different absolute lengths at 18 dpa but the fold change in growth was
297 comparable (Fig. 7E). Also, no significant difference is GR length was detected in regenerates
298 from cut A or D (Fig. 7F). Thus, the inhibitory effect of the head was overcome when enough
299 posterior GR tissue was removed. These results suggest that there are yet more signals to be
300 uncovered that explain how regeneration is promoted and restricted in tapeworms.
301
302 While there is still much to discover, we propose the following working model (Fig. 8A). The head
303 likely produces direct or indirect inhibitor(s) of a posterior signal that we dub factor X. Factor X
304 may be posterior Wnts, other signaling pathways that crosstalk with Wnt signaling or Wnt-
305 independent signals. The head promotes *sfrp* expression, which is necessary to maintain the GR.
306 The posterior GR produces a counteracting signal that results in stable maintenance of the GR
307 length. Factor X acts via *βcat1* to promote proglottid formation. Proglottids only form at sufficient
308 distance from the head where high *βcat1* activity is present. Upon head amputation (Fig. 8B), *sfrp*
309 expression is inhibited causing the posterior boundary of the GR to creep up towards the anterior.
310 Without the head, inhibition of factor X is relieved and overstimulation of *βcat1* results in
311 increased proglottid regeneration until the GR is fully lost.
312
313 Our experiments also demonstrated that cutting within the GR produced highly mixed results,
314 which can now be explained by our model. Tapeworms grown in vitro are adjusting to a new
315 environment and all tissue dimensions change with time. The various amputation schemes within
316 the GR used throughout this paper revealed that depending on the state of signaling gradients from
317 the head and GR, we pushed regeneration competence toward a pro- or anti-regeneration state.
318 When cuts were made "mid" GR at an unfavorable distance from the head (Fig. 8C), inhibition of
319 factor X dominated leading to failure to regenerate proglottids. However, when a minimal
320 fragment was produced (Fig. 8D), perhaps the absence of factor X negates the inhibitory functions
321 of the head. The head could promote establishment of *sfrp* and proper growth of the GR. At a
322 sufficient distance from the head, factor X is now stimulated and can promote proglottid

323 regeneration. The exact players, direct and indirect relationships, as well as additional molecular
324 mechanisms predicted by our working model still need to be tested but the general take-home
325 holds: a balance of pro- and anti-regeneration factors operate in the GR of *H. diminuta*.

326 **Discussion**

327

328 Regenerative abilities vary widely even amongst species that are competent to regenerate. Thus, it
329 is important to understand the factors that both promote and inhibit regeneration. The flatworm
330 phylum offers opportunities to study variations in regenerative abilities. While the free-living
331 planarian *S. mediterranea* can regenerate from almost any amputation fragment, regeneration in
332 *H. diminuta* is far more limited. This study explores how a balance of activating and inhibiting
333 signals operate in the regeneration-competent region: the GR.

334

335 We show that in addition to regenerating proglottids, *H. diminuta* can also regenerate the posterior
336 GR following amputation. However, the challenge of serial amputation within the GR revealed
337 that there are anti-regeneration factors that were previously unknown. By testing amputation
338 schemes at the anterior, we revealed that the head plays at least two seemingly contradictory roles:
339 1) the head promotes GR maintenance and 2) the head inhibits proliferation within the GR and
340 proglottid regeneration. Interestingly, these two roles can be separated both anatomically and
341 through molecular regulators.

342

343 GR maintenance depends on the brain-region without which the GR will eventually be lost. Loss
344 of the GR is gradual unless the anterior GR is also removed. The head likely acts as an organizer
345 that relays signals within the GR. In this model, total loss of the GR will occur after anterior-
346 enriched patterns within the GR turnover and cannot be reestablished following head amputation.
347 One critical mediator of head-dependent GR maintenance is *sfrp*. Like head amputation, RNAi of
348 *sfrp* results in shortened GRs. However, *sfrp* RNAi does not phenocopy the growth spurts observed
349 after head amputation. The mechanism by which *sfrp* maintains the GR is more mysterious. While
350 *sfrp* is primarily known as a Wnt antagonist, it has also been shown to bind and stimulate frizzled
351 receptors, interact with other signaling pathways and modulate cell-matrix interactions by binding
352 integrins (Bovolenta et al., 2008; Mii and Taira, 2011). There is evidence that *sfrps* can stimulate
353 Wnt and BMP signaling in the zebrafish retina (Holly et al., 2014). In Drosophila, *sfrps* can
354 modulate Wnt signaling in a biphasic manner: inhibiting Wnt signaling when expressed at high
355 levels while promoting Wnt signaling when expressed at low levels (Üren et al., 2000). In *H.*
356 *diminuta*, the *sfrp* RNAi phenotypes were not the opposite of the *βcat1* RNAi phenotypes as one

357 might predict if *sfrp* and *βcat1* were acting solely as Wnt antagonist and Wnt effector respectively.
358 Nonetheless, it is still possible that *sfrp* is inhibiting Wnt signaling. In many flatworms, Wnt
359 ligands are secreted from both anterior and posterior domains (Armstrong et al., 2025; Koziol et
360 al., 2016; Reddien, 2018; Soria et al., 2020). Expression of *sfrp* throughout the GR may be required
361 as a permissive signal to tune Wnt signaling to a moderately low level so that it can be acted upon
362 differentially by other modulators. Alternatively, *sfrp* may be functioning independent of Wnt
363 signaling. Future studies investigating the RNAi phenotypes of other Wnt antagonists, Wnt ligands
364 and frizzed receptors will be necessary to determine how Wnt signaling regulates individual cell-
365 and tissue-level behaviors at the GR that are necessary for regeneration.
366
367 A further complication is that the biochemical properties and interactors of SFRP proteins in
368 flatworms in not well understood. Both frizzled and netrin domains are readily identifiable in
369 flatworm SFRPs. The netrin domain should contain 6 conserved cysteine residues (Bhat et al.,
370 2007; Chong et al., 2002) and conflicting conclusions have been asserted as to whether parasitic
371 flatworm SFRPs satisfy this requirement (Armstrong et al., 2025; Koziol et al., 2016; Riddiford
372 and Olson, 2011). Our alignments predict that all 6 cysteine residues are present, however, the 6th
373 residue is displaced by three animo acids in flatworms but not humans (Fig. S5). The three
374 additional amino acids are also present in free living *S. mediterranea* and *Smed-sfrp1* is generally
375 accepted as a Wnt antagonist. While planarian *sfrp* paralogs show complex expression patterns
376 (Gurley et al., 2010), *Smed-sfrp1* is an anterior marker that robustly responds to Wnt inhibition
377 and loss of posterior identity (Doddihal et al., 2024; Hill and Petersen, 2018; Reuter et al., 2015;
378 Scimone et al., 2016; Sureda-Gómez et al., 2015). RNAi of *Smed-sfrp1* shifts the gradient of Smed-
379 βCAT1 protein expression anteriorly supporting *Smed-sfrp1* function as a Wnt antagonist
380 (Stückemann et al., 2017). However, other Wnt antagonists such as *Smed-notum* demonstrate
381 much clearer evidence of Wnt inhibition. *Smed-notum* RNAi results in tail regeneration in place
382 of heads (Petersen and Reddien, 2011) as opposed to *Smed-βcat1* RNAi, which results in head
383 regeneration in place of tails (Gurley et al., 2008; Iglesias et al., 2008; Petersen and Reddien,
384 2008). Thus, it remains possible that a muted or more ambiguous role in Wnt signaling by *sfrp1* is
385 a shared feature in free-living and parasitic flatworms.
386

387 In addition to GR maintenance, the head negatively regulates both proliferation in the GR and
388 proglottid regeneration in a dose-dependent and distance-dependent manner with increased
389 proliferation farther from the head. This observation suggests that the head may be the source of
390 growth inhibitors that diffuse or are differentially received along the A-P axis of the GR. We find
391 that at least one posterior-enriched factor, *βcat1*, is necessary for stem cell maintenance in the GR.
392 Knockdown of *βcat1* results in a dramatic inhibition of growth, proglottid regeneration and
393 ultimately death. Recently, a study in the liver fluke, *Fasciola hepatica,* demonstrated that RNAi
394 of *Fhep-βcat1* resulted in stunted juvenile growth, decreased proliferation and worm death
395 (Armstrong et al., 2025), phenocopying our observations. Thus, roles for *βcat1* in regulating stem
396 cell proliferation and/or survival may be a common theme in parasitic flatworms as it is in many
397 metazoans as well as in neoplastic transformations (Mohammed et al., 2016; Steinhart and Angers,
398 2018) .
399
400 In addition to canonical Wnt signaling, β-catenin proteins have additional roles in cell adhesion
401 through linking cadherins with the actin cytoskeleton via α-catenin. These two functions have been
402 reported in many but not all species. In *S. mediterranea,* there is complete separation of function
403 by two catenin paralogs: Smed-βCAT1 mediates Wnt signaling whereas Smed-βCAT2 mediates
404 cell adhesion (Chai et al., 2010; Su et al., 2017). Accordingly, Smed-βCAT1 does not have α-
405 catenin binding sites (Chai et al., 2010; Su et al., 2017). The presence/absence of α-catenin binding
406 sites in βCAT1 from tapeworms is more ambiguous. Previously, a likely α-catenin binding region
407 demarcated by 10 putative critical residues within a 26 amino acid span was identified for βCAT1
408 and βCAT2 in flatworms (Montagne et al., 2019). The 10 residues were identified as necessary for
409 α-catenin binding to mammalian plakoglobin and/or βcatenin using alanine scanning mutagenesis
410 (Aberle et al., 1996; Pokutta and Weis, 2000). When compared to human βcatenin (CTNB1), we
411 and others find strong conservation of this α-catenin binding region in βCAT2 from multiple
412 flatworms (Fig. S3B) (Montagne et al., 2019). While Smed-βCAT1 is clearly very divergent at
413 this site, two tapeworms (*H. diminuta* and *E. multilocularis*) show more similarity to the human
414 reference (Fig. S3B) (Montagne et al., 2019). Thus, we cannot rule out the possibility that βCAT1
415 in tapeworms functions in both Wnt signaling and cell adhesion, unlike their free-living
416 counterparts. Future studies investigating the biochemical interactions and functional roles of all

417 βcatenin paralogs will help resolve the mechanisms regulating stem cell maintenance in parasitic
418 flatworms.
419
420 The role of *βcat1* in posterior identity is well conserved across many taxa (Petersen and Reddien,
421 2009). In planarian species that are deficient in head regeneration, knockdown of *βcat1* alone can
422 rescue head regeneration indicating that failure to regenerate the head in wild type worms was due
423 to the inability to overcome the posteriorizing effects of *βcat1* (Liu et al., 2013; Sikes and
424 Newmark, 2013; Umesono et al., 2013). *H. diminuta* cannot regenerate its head and we initially
425 assumed that tapeworm *βcat1* would be acting in a homologous fashion to planarians. Because
426 *βcat1* is required for stem cell maintenance in *H. diminuta,* potential roles in posteriorization could
427 not be uncovered. It remains possible that Wnt signaling is necessary to maintain GR posterior
428 identity in *H. diminuta*. Extensive RNAi manipulations of Wnt signaling components that are
429 beyond the scope of this study will help reveal a more holistic understanding of Wnt signaling in
430 this system. However, tapeworms and planarians do differ in that *Smed-βcat1* is not necessary for
431 stem cell maintenance.
432
433 The differences in utilization of *βcat1* between different species of platyhelminths is potentially
434 very interesting. Perhaps segregating functions in posteriorization vs. stem cell maintenance in *S.*
435 *mediterranea* has enabled more nimble remodeling of axes that makes this species so remarkable
436 at regenerating from almost any amputated fragment. In intestinal tapeworms, the head contains
437 suckers that are necessary for attachment without which the tapeworm will simply be extruded
438 with the feces. Thus, maintenance of the head and proglottid regeneration should not be easily
439 decoupled in tapeworms. Considering the wider role for βcatenin in regulating stem cell
440 proliferation and survival across metazoa, it would be easy to suppose that planarian phenotype is
441 divergent. However, studies in the acoel *Hofstenia miamia*, a representative of a sister taxa to all
442 bilaterians, show that RNAi of *Hmia-βcat1* is necessary for maintaining posterior identity but
443 functions in regulating stem cells, proliferation, or growth were not reported (Srivastava et al.,
444 2014; Tewari et al., 2019). Considering that *Hmia-βcat1* RNAi experiments were performed in the
445 context of regeneration, inhibition of growth is unlikely to have been missed with the caveat the
446 RNAi cannot be fully penetrant. Thus, there is evidence that the planarian phenotype is ancestral.

447 A deeper understanding of how catenin paralogs have evolved across platyhelminths and how they
448 have functionally specialized will be illuminating. Such investigations would enrich our
449 understanding of how strategies to regulate axial identity and stem cell proliferation/survival have
450 evolved in regeneration-competent species.
451
452 Our work has revealed that a balance of opposing signals from anterior and posterior ends of the
453 GR are necessary for proper regeneration. It makes intuitive sense that initiation of proglottids
454 must be inhibited close to the head if the GR is to be maintained as an unsegmented tissue. A
455 recent study from the mouse bile duct tapeworm, *Hymenolepis microstoma,* has described discrete
456 expression of Wnt and Hedgehog signaling components in a signaling quartet (SQ) within the
457 transition zone from GR to fully elaborated proglottids (Jarero et al., 2024). It is possible the SQ
458 initiates proglottid formation and represents the unknown X factor predicted by our study. How
459 the SQ responds to head-dependent signals and vice versa is currently unknown and warrants
460 future investigation.
461
462 Our study also shows that regulation of proliferation dynamics is dependent on signals from the
463 head. Why should the head provide anti-proliferation signals at all? One intriguing possibility is
464 that distinct subpopulations of stem cells within the GR respond differentially to signals from the
465 head. Such signals may affect the balance of self-renewal vs. differentiation. Alternatively, a slow-
466 cycling pluri- or multi-potent subpopulation of stem cells may require these head-dependent
467 signals. There is already evidence for different cycling rates in stem cells of parasitic flatworms
468 (Herz et al., 2024; Wang et al., 2018) . In this study, we observed that amputations made
469 progressively closer to the head inhibited regeneration until enough posterior GR tissue was
470 removed, which restored competence to regenerate. Perhaps the anterior portion of the GR contains
471 the minimal cohort of stem cells required to regenerate the GR and seed new proglottids. These
472 anterior stem cells may represent a slow-cycling population with greater potency. These ideas are
473 highly speculative, but investigating how head-dependent signals impact stem cell subpopulations
474 in the GR may shed light on the regulation of stem cell potency in tapeworms and potentially other
475 species.

476 **Materials and Methods**

477

478 Animal care and use

479 The life cycle of *H. diminuta* was maintained in house using mealworm beetles (*Tenebrio molitor*)
480 and Sprague-Dawley rats for the larval and adult stages respectively. Rats were fed 200-400
481 infective cysticercoids by oral gavage in ~0.5 mL 0.85% NaCl. Typically, adult tapeworms were
482 collected 6 days post infection by euthanizing infected rats in a CO_2 chamber and flushing the
483 small intestine with 1X Hanks Balanced Salt Solution (HBSS: 21-023-CV; Corning). Rodent care
484 was performed in accordance with protocols approved by the Institutional Animal Care and Use
485 Committee (IACUC) of the University of Georgia (A2023 10-019-Y1-A0).

486

487 In vitro parasite culture

488 Adult tapeworms or amputated fragments were grown in vitro in biphasic cultures as described
489 before (Rozario et al., 2019). 2.5X MEM essential amino acids (M5550; Sigma-Aldrich) was
490 added to the liquid culture: Working Hanks 4 (WH4: HBSS/4 g/L glucose/antibiotic-antimycotic).
491 This ameliorated inconsistencies between batches of blood used for culturing but was not strictly
492 necessary.

493

494 In situ hybridization and other staining

495 Heat-kills were performed by swirling tapeworms in 75°C water for a few seconds before fixing
496 (4% formaldehyde in Phosphate Buffered Saline with 0.3% TritonX-100 (PBSTx)) for 30 min-2
497 hr at room temperature or overnight at 4°C. Worms were either dehydrated into methanol and
498 stored (-30°C) or used directly for staining. For simple phenotyping of growth and regeneration,
499 worms were stained in 1 μg/mL DAPI (D9542; Sigma-Aldrich)/PBSTx overnight at 4°C and
500 cleared in mounting solution (80% glycerol/10 mM Tris pH7.5/ 1 mM EDTA) overnight before
501 mounting and imaging. Previously published methods were employed for in situ hybridization
502 (Rozario et al., 2019) and immunostaining (Rozario and Newmark, 2015). Anti-Syn antibodies
503 (3C11; Developmental Studies Hybridoma Bank) were used at 1:200 with Tyramide Signal
504 Amplification (TSA).

505

506 F-*ara*-EdU uptake and staining

507 F-*ara*-EdU pulses were performed in 0.1 μM F-*ara*-EdU (T511293; Sigma-Aldrich)/1%
508 DMSO/WH4 at 37°C for 1 hr. Staining was performed as previously described (Ishan et al., in
509 press) with the following specifics: 1) 15 min proteinase-K digestion and 2) 10 min TSA reaction.
510
511 Imaging and image processing
512 Confocal imaging was performed on a Zeiss LSM 900 with the following objectives: 20X/Plan-
513 Apochromat/0.8 M27/FWD=0.55mm and 63X/Plan-Apochromat/1.40 Oil DIC M27. WISH and
514 DAPI-stained worms were imaged on a Zeiss AxioZoom V16 Microscope. Fiji (Schindelin et al.,
515 2012) was used for brightness/contrast adjustments, maximum-intensity projections and
516 measurements of lengths, areas, and numbers of proglottids. F-*ara*-EdU+ cells were quantified
517 using Imaris (Oxford Instruments) spot finder as previously described (Ishan et al., in press) .
518
519 RNAi
520 To perform knockdowns, tapeworms were microinjected with dsRNA (1-1.5 μg/μl in HBSS), 2
521 mm anterior fragments were amputated 3 days later and cultured in vitro. Injections were
522 performed using a Femtojet 4i (Eppendorf) at 500 hPa for 0.3-1s. dsRNA was synthesized as
523 previously described (Rouhana et al., 2013) from ~1 kb PCR products from cDNA cloned into
524 pJC53.2 vector (Collins et al., 2010). Experimenters were blinded to the dsRNA used throughout
525 microinjections, staining and image analysis.
526
527 qRT-PCR
528 To exclude genomic DNA, primers were designed to flank introns or span an intron-exon junction.
529 Amplicon range was 133-277 bp. All primers were tested on cDNA +/- reverse transcriptase and
530 gel electrophoresis to confirm the presence of a single product. Primer efficiencies were calculated
531 from 2-fold serial dilutions of cDNA.
532
533 For RNA extractions, 3 mm anteriors from 4-5 worms were cut, submerged in 200 μL TRIzol
534 Reagent (15596026; Invitrogen) and processed according to manufacturer's instructions with these
535 exceptions: 1) samples were homogenized with a motorized pestle twice in a semi-solid state then
536 centrifuged at >12K RCF for 5 min to obtain 180 μL clean supernatant, 2) RNA pellets were
537 washed twice with 75% ethanol-DEPC and 3); pellets were resuspended in 40 μL nuclease-free

538 water. DNAse (M6101; Promega) treatment was performed for 1 hr at 37°C. RNA was cleaned
539 using RNA Clean & Concentrator-5 kit (R1016; Zymo Research) and the concentration measured
540 on a Nanodrop spectrophotometer. cDNA synthesis was performed, according to manufacturer's
541 protocol, using Oligo$(dT)_{20}$ primers and iScript Select cDNA Synthesis Kit (1708897; Bio-Rad)
542 with undiluted RNA. cDNA was further diluted with 5-25 µL nuclease-free water depending on
543 the number of reactions needed.
544
545 qRT-PCR was performed using GoTaq MasterMix (A6001; Promega) according to manufacturer's
546 instructions and scaled to 25 µL reactions with 2 µL cDNA template for each of 3 technical
547 replicates. Each reaction had 0.4 µM primer pairs, 0.3 µM CXCR in 1X master mix. 7500 Real
548 Time PCR System (Applied Biosystems) was used for 40 amplification cycles: 15 s at 95°C and 1
549 min at 60°C. Relative gene expression change was calculated using the PFAFFL equation
550 (Hellemans et al., 2007; Vandesompele et al., 2002) to account for different primer efficiencies.
551 Internal normalization was done on the geometric mean of two previously published standards:
552 *60S ribosomal protein L13* (*60Srpl13*) and *myosin heavy chain* (*mhc*) (Rozario et al., 2019) .
553
554 Statistical Analysis
555 Graph Pad Prism 10 was used for all statistical analyses. All experiments were repeated at least
556 twice. Error bars, statistical tests, number of replicates (N) and sample sizes (n) are indicated in
557 corresponding figure legends. P-values: ns = not significant, * = $p<0.05$, **=$p<0.01$, ***=$p<0.001$,
558 ****=$p<0.0001$.
559

Acknowledgements

We are sincerely thankful to Phil Newmark and Melanie Issigonis (Morgridge Institute for Research, WI). Phil's unwavering support in the initialization of these projects and continued advice was instrumental in our success. We are also grateful for Melanie's critical evaluation of our manuscript and valuable feedback. We thank the Biomedical Microscopy Core at the University of Georgia, Athens, GA for necessary microscopy services.

Competing interests

No conflicts to report.

Funding

This work was funded by a National Institute of Allergy and Infectious Disease (NIAID) grant (DP2 AI 154416-01) to Tania Rozario.

Data and resource availability

All relevant data and resources can be found within the article and its supplementary information. Primers and transcripts used are listed in Table S2. All source data is provided in Table S3.

577 **References**

578 **Aberle, H., Schwartz, H., Hoschuetzky, H. and Kemler, R.** (1996). Single Amino Acid
579 Substitutions in Proteins of the armadillo Gene Family Abolish Their Binding to α-Catenin
580 (∗). *J. Biol. Chem.* **271**, 1520–1526.

581 **Armstrong, R., Marks, N. J., Geary, T. G., Harrington, J., Selzer, P. M. and Maule, A. G.**
582 (2025). Wnt/β-catenin signalling underpins juvenile *Fasciola hepatica* growth and
583 development. *PLOS Pathog.* **21**, e1012562.

584 **Bely, A. E. and Nyberg, K. G.** (2010). Evolution of animal regeneration: re-emergence of a
585 field. *Trends in Ecology & Evolution* **25**, 161–170.

586 **Bhat, R. A., Stauffer, B., Komm, B. S. and Bodine, P. V. N.** (2007). Structure–Function
587 analysis of secreted frizzled-related protein-1 for its Wnt antagonist function. *J. Cell.*
588 *Biochem.* **102**, 1519–1528.

589 **Blum, M., Chang, H.-Y., Chuguransky, S., Grego, T., Kandasaamy, S., Mitchell, A., Nuka,**
590 **G., Paysan-Lafosse, T., Qureshi, M., Raj, S., et al.** (2020). The InterPro protein families
591 and domains database: 20 years on. *Nucleic Acids Res.* **49**, D344–D354.

592 **Bovolenta, P., Esteve, P., Ruiz, J. M., Cisneros, E. and Lopez-Rios, J.** (2008). Beyond Wnt
593 inhibition: new functions of secreted Frizzled-related proteins in development and disease. *J.*
594 *Cell Sci.* **121**, 737–746.

595 **Chai, G., Ma, C., Bao, K., Zheng, L., Wang, X., Sun, Z., Salò, E., Adell, T. and Wu, W.**
596 (2010). Complete functional segregation of planarian β-catenin-1 and -2 in mediating Wnt
597 signaling and cell adhesion. *The Journal of biological chemistry* **285**, 24120–24130.

598 **Chong, J. M., Üren, A., Rubin, J. S. and Speicher, D. W.** (2002). Disulfide Bond Assignments
599 of Secreted Frizzled-related Protein-1 Provide Insights about Frizzled Homology and Netrin
600 Modules. *J. Biol. Chem.* **277**, 5134–5144.

601 **Collins, J. J., Hou, X., Romanova, E. V., Lambrus, B. G., Miller, C. M., Saberi, A.,**
602 **Sweedler, J. V. and Newmark, P. A.** (2010). Genome-wide analyses reveal a role for
603 peptide hormones in planarian germline development. *PLoS biology* **8**, e1000509.

604 **Doddihal, V., Mann, F. G., Ross, E. J., McKinney, M. C., Guerrero-Hernández, C.,**
605 **Brewster, C. E., McKinney, S. A. and Alvarado, A. S.** (2024). A PAK family kinase and
606 the Hippo/Yorkie pathway modulate WNT signaling to functionally integrate body axes
607 during regeneration. *Proc. Natl. Acad. Sci.* **121**, e2321919121.

608 **Goodchild, C. G.** (1958). Transfaunation and Repair of Damage in the Rat Tapeworm,
609 *Hymenolepis diminuta*. *The Journal of parasitology* **44**, 345–351.

610 **Gurley, K. A., Rink, J. C. and Alvarado, A. S.** (2008). β-catenin defines head versus tail
611 identity during planarian regeneration and homeostasis. *Science* **319**, 323–327.

612 **Gurley, K. A., Elliott, S. A., Simakov, O., Schmidt, H. A., Holstein, T. W. and Alvarado, A.**
613 **S.** (2010). Expression of secreted Wnt pathway components reveals unexpected complexity of
614 the planarian amputation response. *Developmental biology* **347**, 24–39.

615 **Hellemans, J., Mortier, G., Paepe, A. D., Speleman, F. and Vandesompele, J.** (2007). qBase
616 relative quantification framework and software for management and automated analysis of
617 real-time quantitative PCR data. *Genome Biol.* **8**, R19.

618 **Herz, M., Zarowiecki, M., Wessels, L., Pätzel, K., Herrmann, R., Braun, C., Holroyd, N.,**
619 **Huckvale, T., Bergmann, M., Spiliotis, M., et al.** (2024). Genome-wide transcriptome
620 analysis of *Echinococcus multilocularis* larvae and germinative cell cultures reveals genes
621 involved in parasite stem cell function. *Front. Cell. Infect. Microbiol.* **14**, 1335946.

622 **Hill, E. M. and Petersen, C. P.** (2018). Positional information specifies the site of organ
623 regeneration and not tissue maintenance in planarians. *eLife* **7**, e02238.

624 **Holly, V. L., Widen, S. A., Famulski, J. K. and Waskiewicz, A. J.** (2014). Sfrp1a and Sfrp5
625 function as positive regulators of Wnt and BMP signaling during early retinal development.
626 *Dev. Biol.* **388**, 192–204.

627 **Iglesias, M., Gomez-Skarmeta, J. L., Saló, E. and Adell, T.** (2008). Silencing of *Smed-*
628 *βcatenin1* generates radial-like hypercephalized planarians. *Development* **135**, 1215–1221.

629 **Ishan, M., Skipper, I. R. and Rozario, T.** (2025). Combined fluorescent in situ hybridization
630 and F-ara-EdU staining on whole mount *Hymenolepis diminuta*. *Biol. Methods Protoc.*
631 bpaf011. (in press)

632 **Jarero, F., Baillie, A., Riddiford, N., Montagne, J., Koziol, U. and Olson, P. D.** (2024).
633 Muscular remodeling and anteroposterior patterning during tapeworm segmentation. *Dev.*
634 *Dyn.* **253**: 998–1023.

635 **Koziol, U., Jarero, F., Olson, P. D. and Brehm, K.** (2016). Comparative analysis of Wnt
636 expression identifies a highly conserved developmental transition in flatworms. *BMC biology*
637 **14**, 1.

638 **Laumer, C. E., Hejnol, A. and Giribet, G.** (2015). Nuclear genomic signals of the
639 "microturbellarian" roots of platyhelminth evolutionary innovation. *eLife* **4**, e05503.

640 **Leyns, L., Bouwmeester, T., Kim, S.-H., Piccolo, S. and Robertis, E. M. D.** (1997). Frzb-1 Is
641 a Secreted Antagonist of Wnt Signaling Expressed in the Spemann Organizer. *Cell* **88**, 747–
642 756.

643 **Liu, S. Y., Selck, C., Friedrich, B., Lutz, R., Vila-Farré, M., Dahl, A., Brandl, H.,**
644 **Lakshmanaperumal, N., Henry, I. and Rink, J. C.** (2013). Reactivating head regrowth in a
645 regeneration-deficient planarian species. *Nature* **500**, 81–84.

646 **Mii, Y. and Taira, M.** (2011). Secreted Wnt "inhibitors" are not just inhibitors: Regulation of
647 extracellular Wnt by secreted Frizzled-related proteins. *Dev., Growth Differ.* **53**, 911–923.

648 **Mohammed, M. K., Shao, C., Wang, J., Wei, Q., Wang, X., Collier, Z., Tang, S., Liu, H.,**
649 **Zhang, F., Huang, J., et al.** (2016). Wnt/β-catenin signaling plays an ever-expanding role in
650 stem cell self-renewal, tumorigenesis and cancer chemoresistance. *Genes Dis.* **3**, 11–40.

651 **Montagne, J., Preza, M., Castillo, E., Brehm, K. and Koziol, U.** (2019). Divergent Axin and
652 GSK-3 paralogs in the beta-catenin destruction complexes of tapeworms. *Development genes*
653 *and evolution* **11**, 1–14.

654 **Nusse, R. and Clevers, H.** (2017). Wnt/β-Catenin Signaling, Disease, and Emerging
655 Therapeutic Modalities. *Cell* **169**, 985–999.

656 **Petersen, C. P. and Reddien, P. W.** (2008). *Smed-βcatenin-1* is required for anteroposterior
657 blastema polarity in planarian regeneration. *Science* **319**, 327–330.

658 **Petersen, C. P. and Reddien, P. W.** (2009). Wnt signaling and the polarity of the primary body
659 axis. *Cell* **139**, 1056–1068.

660 **Petersen, C. P. and Reddien, P. W.** (2011). Polarized notum activation at wounds inhibits Wnt
661 function to promote planarian head regeneration. *Science* **332**, 852–855.

662 **Pokutta, S. and Weis, W. I.** (2000). Structure of the Dimerization and β-Catenin- Binding
663 Region of α-Catenin. *Mol. Cell* **5**, 533–543.

664 **Rattner, A., Hsieh, J.-C., Smallwood, P. M., Gilbert, D. J., Copeland, N. G., Jenkins, N. A.**
665 **and Nathans, J.** (1997). A family of secreted proteins contains homology to the cysteine-rich
666 ligand-binding domain of frizzled receptors. *Proc. Natl. Acad. Sci.* **94**, 2859–2863.

667 **Read, C. P.** (1967). Longevity of the tapeworm, *Hymenolepis diminuta*. *J Parasitol* **53**, 1055–6.

668 **Reddien, P. W.** (2018). The Cellular and Molecular Basis for Planarian Regeneration. *Cell* **175**,
669 327–345.

670 **Reuter, H., März, M., Vogg, M. C., Eccles, D., Grífol-Boldú, L., Wehner, D., Owlarn, S.,**
671 **Adell, T., Weidinger, G. and Bartscherer, K.** (2015). β-Catenin-Dependent Control of
672 Positional Information along the AP Body Axis in Planarians Involves a Teashirt Family
673 Member. *Cell reports* **10**, 253–265.

674 **Riddiford, N. and Olson, P. D.** (2011). Wnt gene loss in flatworms. *Development genes and*
675 *evolution* **221**, 187–197.

676 **Rouhana, L., Weiss, J. A., Forsthoefel, D. J., Lee, H., King, R. S., Inoue, T., Shibata, N.,**
677 **Agata, K. and Newmark, P. A.** (2013). RNA interference by feeding in vitro-synthesized
678 double-stranded RNA to planarians: methodology and dynamics. *Dev. Dyn.* **242**, 718–730.

679 **Rozario, T. and Newmark, P. A.** (2015). A confocal microscopy-based atlas of tissue
680 architecture in the tapeworm *Hymenolepis diminuta*. *Experimental parasitology* **158**, 31–41.

681 **Rozario, T., Quinn, E. B., Wang, J., Davis, R. E. and Newmark, P. A.** (2019). Region-
682 specific regulation of stem cell-driven regeneration in tapeworms. *eLife* **8**, e48958.

683 **Schindelin, J., Arganda-Carreras, I., Frise, E., Kaynig, V., Longair, M., Pietzsch, T.,**
684 **Preibisch, S., Rueden, C., Saalfeld, S., Schmid, B., et al.** (2012). Fiji: an open-source
685 platform for biological-image analysis. *Nat. Methods* **9**, 676–682.

686 **Scimone, M. L., Cote, L. E., Rogers, T. and Reddien, P. W.** (2016). Two FGFRL-Wnt circuits
687 organize the planarian anteroposterior axis. *eLife* **5**, 905.

688 **Sikes, J. M. and Newmark, P. A.** (2013). Restoration of anterior regeneration in a planarian
689 with limited regenerative ability. *Nature* **500**, 77–80.

690 **Soria, C. L. D., Lee, J., Chong, T., Coghlan, A., Tracey, A., Young, M. D., Andrews, T.,**
691 **Hall, C., Ng, B. L., Rawlinson, K., et al.** (2020). Single-cell atlas of the first intra-
692 mammalian developmental stage of the human parasite *Schistosoma mansoni*. *Nat. Commun.*
693 **11**, 6411.

694 **Srivastava, M., Mazza-Curll, K. L., Wolfswinkel, J. C. van and Reddien, P. W.** (2014).
695 Whole-Body Acoel Regeneration Is Controlled by Wnt and Bmp-Admp Signaling. *Current*
696 *biology : CB* **24**, 1107–1113.

697 **Steinhart, Z. and Angers, S.** (2018). Wnt signaling in development and tissue homeostasis.
698 *Development* **145**, dev146589.

699 **Stückemann, T., Cleland, J. P., Werner, S., Vu, H. T.-K., Bayersdorf, R., Liu, S.-Y.,**
700 **Friedrich, B., Jülicher, F. and Rink, J. C.** (2017). Antagonistic Self-Organizing Patterning
701 Systems Control Maintenance and Regeneration of the Anteroposterior Axis in Planarians.
702 *Developmental cell* **40**, 248-263.e4.

703 **Su, H., Sureda-Gomez, M., Rabaneda-Lombarte, N., Gelabert, M., Xie, J., Wu, W. and**
704 **Adell, T.** (2017). A C-terminally truncated form of β-catenin acts as a novel regulator of
705 Wnt/β-catenin signaling in planarians. *PLoS Genet.* **13**, e1007030.

706 **Sureda-Gómez, M., Pascual-Carreras, E. and Adell, T.** (2015). Posterior Wnts Have Distinct
707 Roles in Specification and Patterning of the Planarian Posterior Region. *International journal*
708 *of molecular sciences* **16**, 26543–26554.

709 **Tewari, A. G., Owen, J. H., Petersen, C. P., Wagner, D. E. and Reddien, P. W.** (2019). A
710 small set of conserved genes, including *sp5* and *Hox*, are activated by Wnt signaling in the
711 posterior of planarians and acoels. *PLoS Genet.* **15**, e1008401.

712 **Umesono, Y., Tasaki, J., Nishimura, Y., Hrouda, M., Kawaguchi, E., Yazawa, S.,**
713 **Nishimura, O., Hosoda, K., Inoue, T. and Agata, K.** (2013). The molecular logic for
714 planarian regeneration along the anterior-posterior axis. *Nature* **500**, 73–76.

715 **Üren, A., Reichsman, F., Anest, V., Taylor, W. G., Muraiso, K., Bottaro, D. P.,**
716 **Cumberledge, S. and Rubin, J. S.** (2000). Secreted Frizzled-related Protein-1 Binds Directly
717 to Wingless and Is a Biphasic Modulator of Wnt Signaling*. *J. Biol. Chem.* **275**, 4374–4382.

718 **Valenta, T., Hausmann, G. and Basler, K.** (2012). The many faces and functions of β-catenin.
719 *EMBO J.* **31**, 2714–2736.

720 **Vandesompele, J., Preter, K. D., Pattyn, F., Poppe, B., Roy, N. V., Paepe, A. D. and**
721 **Speleman, F.** (2002). Accurate normalization of real-time quantitative RT-PCR data by
722 geometric averaging of multiple internal control genes. *Genome Biol.* **3**, research0034.1.

723 **Wang, S., Krinks, M., Lin, K., Luyten, F. P. and Moos, M.** (1997). Frzb, a Secreted Protein
724 Expressed in the Spemann Organizer, Binds and Inhibits Wnt-8. *Cell* **88**, 757–766.

Wang, B., Lee, J., Li, P., Saberi, A., Yang, H., Liu, C., Zhao, M. and Newmark, P. A. (2018). Stem cell heterogeneity drives the parasitic life cycle of *Schistosoma mansoni*. *eLife* **7**, e35449.

729 **Figure legends**

730

731 **Fig. 1. The germinative region (GR) regenerates after a single amputation.** (A) DAPI-stained
732 images of anterior fragments cut within the GR (0.5 mm) or outside of it (2 mm) at 15 dpa.
733 Quantification of growth in length and number of proglottids regenerated at 15 dpa. N=3, n= 6-10
734 per condition; t-test. (B) DAPI-stained image of 0.5 mm anterior fragment at 15 dpa showing
735 regenerated GR. Yellow arrowhead marks the first proglottid. Quantification of GR lengths from
736 A; t-test. (C) Quantification of proglottids regenerated and length every 2 days from 0.5 mm vs. 2
737 mm anterior fragments. Change in proglottids was fitted with a simple linear regression and
738 showed 14-15 proglottids regenerated per day. Change in length was fitted with a nonlinear curve
739 as each proglottid increases in length. n=5-7 fragments per group per timepoint. (D) WISH for
740 transcripts with A-P polarized expression patterns 3 days after acclimation to in vitro culture
741 (uncut, n = 7-10 per transcript) then amputated at 0.5 mm and stained at 0 dpa (n= 7-8 per
742 transcript) and 10 dpa (n= 5-13 per transcript). Asterisks mark pigmented debris that adhered to
743 cut ends. Error bars= SD.

744

745 **Fig. 2. Serial amputation within the GR negatively affects regenerative ability.** (A) Scheme
746 for serial amputation within the GR. (B-C) GR lengths and percentage of GR retained compared
747 to uncut whole worms at 0 dpa. n=7-10 per timepoint per experiment. (D) DAPI-stained
748 regenerates 18 dpa for each cut. (E-F) Quantification of regeneration success rate and number of
749 proglottids regenerated (n= 8-10 per timepoint per experiment). Error bars= SD; t-test.

750

751 **Fig. 3. The head inhibits proglottid regeneration and cell proliferation.** (A) DAPI-stained
752 regenerates from 0.5 mm amputations +/- head at 15 dpa. Quantification of proglottids regenerated
753 from a representative experiment. n= 7; t-test. (B) Confocal micrographs from maximum intensity
754 projections of +/- head worms at 3 dpa immunostained for neuronal marker SYN after a 1 hr pulse
755 of F-*ara*-EdU to label proliferating cells. Quantification of the density of proliferating cells within
756 the GR from a representative experiment. Each sample was normalized to the mean proliferation
757 density in the corresponding +head group. n= 5-6 per group per timepoint; t-test. (C-D) Maximum
758 intensity projections of worm anteriors after 1 hr pulse of F-*ara*-EdU either with the head (C) or -
759 head 3 dpa (D). Yellow dotted lines represent 200 μm-wide regions used for quantification of

760 proliferation density. H= head. Quantification across 3 cohorts, n=11 and 13; one-way ANOVA
761 with Dunnett's multiple testing correction. Error bars= SD.
762
763 **Fig. 4. Effect of head or head-adjacent amputations on proliferation and regeneration.** (A)
764 Scheme for results shown in B-C and Fig. S2. Step 1: Four amputation schemes were tested: intact
765 head (+head), transverse cut through half the head while retaining the brain (½ head), full head
766 amputation (-head) and cut 0.5 mm from the anterior into the GR (-0.5 mm). Step 2: all worms
767 were amputated posteriorly to obtain 2 mm fragments. Step 3: fragments were grown in vitro for
768 14 days. Step 4-5: regenerates were collected and recut to obtain 2 mm anterior fragments that
769 were cultured in vitro while the posteriors were fixed and stained with DAPI to measure the
770 number of proglottids regenerated. (B) Quantification of proglottids regenerated. All samples were
771 normalized to the mean of the +head worms set to 100%. Bars indicate the means from 2-3
772 experiments for all samples after cut 1 and only for samples with visible GRs for cut 2-4. Fully
773 proglottidized worms without a GR are represented with a red dot. (C) Percentage of regenerates
774 that still maintained a visible GR from B. (D) After cut 4, proglottids regenerated from +head and
775 ½ head samples from one experiment were plotted against the area of the head remaining measured
776 from DAPI stained worms. Linear regression fitted. (E-F) Quantification of F-*ara*-EdU+ cells
777 normalized to area within the GR 3 dpa. All samples were normalized to the mean of the +head
778 worms set to 100%. Means from 3-4 experiments analyzed with two-way ANOVA (mixed model)
779 and Tukey's multiple corrections test (E). All pooled data from analyzed with one-way ANOVA
780 compared to +head with Dunnett's multiple comparison test (n= 21-28). Error bars= SD.
781
782 **Fig. 5. *βcat1* is a posterior-biased factor that is necessary to maintain the cycling stem cell**
783 **population in the GR.** (A) Schematic and WISH of *βcat1* expression at the GR from a wild type
784 6-day-old adult. (B) DAPI-stained 2 mm anterior regenerates after single injection of dsRNA at 7
785 dpa. (C) Quantification of worm lengths after RNAi at 7 dpa. Bars show means and grey circles
786 represent individual worms. N= 3, n= 23-24 per group; one-way ANOVA with Dunnett's multiple
787 comparison test. (D) qRT-PCR from 3 RNAi experiments. Target expression normalized to two
788 endogenous controls and compared to *GFP* RNAi set at 1 (dotted line). (E) Representative
789 maximum intensity confocal projections at the GR stained after 1 hr F-*ara*-EdU uptake. Dotted
790 yellow lines are the worm outlines. Quantification of F-*ara*-EdU+ cells normalized to area within

791 an 800 μm-wide cropped region directly posterior to the head at 6-7 dpi. All samples were
792 normalized to the mean of *GFP* RNAi worms set to 100%. Bars show means and grey circles
793 represent individual worms. N= 3, n= 16-20 per group; one-way ANOVA with Dunnett's multiple
794 comparison test. (F) WISH for cycling stem cell markers *mcm2* and *lbr* at 6 dpi (N=3). Error bars=
795 SD.
796
797 **Fig. 6. *sfrp* is an anterior-biased factor that regulates GR length.** (A) Schematic and WISH of
798 *sfrp* expression at the GR from a wild type 6-day-old adult. (B) RNAi scheme for C-F. Double
799 injections of dsRNA were performed into the head and 2 mm anterior fragments were allowed to
800 regenerate for 10-12 days. (C) Representative DAPI-stained regenerates after RNAi. (D)
801 Quantification of proglottids regenerated after RNAi normalized to mean from *GFP* RNAi set to
802 100%. Bars show means and grey circles represent individual worms. N= 3, n= 25-26 per group;
803 one-way ANOVA with Dunnett's multiple comparison test. (E) Representative DAPI-stained
804 images showing GR lengths (between yellow arrowheads) after RNAi. (F) Quantification of GR
805 lengths from D. Bars show means and grey circles represent individual worms; one-way ANOVA
806 with Dunnett's multiple comparison test. (G) qRT-PCR for *sfrp* expression normalized to two
807 endogenous controls compared +head set at 1. N=3; t-test. Error bars= SD.
808
809 **Fig. 7. How amputations at increasing distance from the head influence competence to**
810 **regenerate.** (A) Regenerates from 0.5 mm anterior fragments were grown for 18 days then
811 amputated a second time at 1 mm (cut A). A subset was fixed to quantify GR length and a subset
812 was grown in vitro for 18 days. The remaining fragments were cut again to shave off ~20-25%
813 more GR (cut B) and the process repeated successively for cut C and cut D. Darkfield images
814 showing the live fragments before transfer to in vitro culture show that the wound site is
815 progressively closer to the head with successive cuts. (B) GR lengths of each fragment measured
816 from DAPI-stained 0 dpa fragments and represented as a percentage of the GR relative to uncut
817 worms from the same cohort. N=3, n= 3-9; one-way ANOVA. (C) Percent of fragments that
818 regenerated proglottids after 18 days from 3 experiments. Each experiment represented by the
819 same color in B and C. (D-F) Comparisons of worm length (D), growth fold change (E) and GR
820 length (F). N=3, n= 20 and 17; t-test. Error bars = SD.
821

822 **Fig. 8. Models for regeneration in *H. diminuta*.** (A) Working model for a minimal complement
823 of factors within the GR. X represents unknown factor(s) that directly/indirectly promote *βcat1*
824 activity. (B-D) Graphical representation using the working model to explain three scenarios
825 described in this study. For all: solid black activating or inhibiting arrows indicate activity in situ
826 whereas dotted grey arrows indicate the associated function without spatial reference.
827
828 **Fig. S1. Proliferation response at wound site.** Worms were amputated at 0.5 mm within the GR.
829 Fragments were analyzed at both the posterior-facing wound (Pfw) and anterior-facing wound
830 (Afw) at 1 dpa following a 1 hr pulse of F-*ara*-EdU. Proliferation density was quantified from a
831 box width of 100 μm from the cut site to capture the local proliferation response to amputation.
832 Quantification from one representative experiment is shown, n= 5-7; error bars= SD, one-way
833 ANOVA with Tukey's multiple testing correction.
834
835 **Fig. S2. How head tissues influence regeneration.** (A) Widefield fluorescent images of ½ head
836 fragments at 0 dpa stained with anti-SYN antibodies. Yellow arrowheads point to the
837 brain/cephalic ganglia. (B) GR lengths at the end of a representative serial amputation experiment.
838 n= 5-8; one-way ANOVA with Dunnett's multiple comparison test. (C) Quantification of
839 proglottids regenerated after cut 1, normalized to +head means. N=3; n=7-17; statistical
840 significance for each of 3 experiments calculated using one-way ANOVA and was the same for
841 all 3. (D) Quantification of proglottids regenerated normalized to +head means. N=2-3, n=5-16;
842 means (black circles) and statistical significance for each experiment using t-test are shown. Error
843 bars= SD.
844
845 **Fig. S3. Domain analysis of *H. diminuta* βCAT1.** (A) Sequence alignment of βCAT1 from four
846 flatworm species (*Hd: H. diminuta, Em: E. multilocularis, Sm: S. mansoni, Smed: S.*
847 *mediterranea*). The conserved DSGxxSxxx[S/T]xxxS motif for CKI/GSK-phosphorylation (red)
848 is present as are armadillo repeats (lilac). The boundaries of both domains are shown according to
849 *S. mediterranea* (Su et al., 2017). The shading indicates identical residues between 4 species (grey)
850 or 3 species (blue). The N- and C-termini are more divergent between all species. (B) Sequence
851 alignment of 26 amino acids covering a putative α-catenin binding domain previously reported
852 (Montagne et al., 2019). 10 critical residues for α-catenin binding (Aberle et al., 1996; Pokutta and

853 Weis, 2000) are marked by the symbol α (green). In reference to human CTNB1, dark grey shading
854 highlights identical residues. Chemically similar residues marked in light grey for aromatic (F, Y,
855 W, H), aliphatic (V, I, L), positively charged (R, K, H), negatively charged (D, E), polar but not
856 charged (N, Q, T, S, Y, C) and hydrophobic (V, I, L, M, A, F, P, W, G) residues, also in reference
857 to human CTNB1.
858
859 **Fig. S4. Wild type WISH expression patterns for *βcat1* and *sfrp*.** Representative micrographs
860 spanning different stages of development in 6-day-old worms with anterior facing left.
861
862 **Fig. S5. Domain analysis of *H. diminuta* SFRP.** BLASTp alignment of SFRPs from flatworms
863 and human SFRP-1,-2 and -5 as references (*Hd: H. diminuta, Em: E. multilocularis, Smed: S.*
864 *mediterranea*). The frizzled domain (orange) and netrin domain (blue) are marked at the most
865 inclusive positions reported for human SFRP1 using Interpro (Blum et al., 2020). Conserved
866 cysteines are highlighted in yellow.
867
868 **Fig. S6. Phenotypes observed after *sfrp* RNAi.** (A) Scheme for RNAi with dsRNA injections
869 throughout the GR. (B-C) Quantification of proglottid regeneration (B) and GR length (C) from
870 two independent experiments; one-way ANOVA with Dunnett's multiple comparison test. (D)
871 Quantification of F-*ara*-EdU+ cells normalized to area within an 800 μm-wide cropped region
872 directly posterior to the head or to the first proglottid. Combined from single and double injections
873 of dsRNA throughout the GR all from experiments with significant *sfrp* knockdown. All samples
874 were normalized to the mean of *GFP* RNAi worms set to 100%. Bars show means and grey circles
875 represent individual worms. N= 3, n= 21-23 per group; one-way ANOVA with Dunnett's multiple
876 comparison test. (E) qRT-PCR from 3 RNAi experiments where dsRNA was injected at the scolex
877 (Sc-biased) or throughout the GR. Expression of *sfrp* was normalized to two endogenous controls
878 compared to *GFP* RNAi set at 1 (dotted line). Error bars= SD.
879
880 **Fig. S7. Comparison of regenerates from longest (cut A) vs. shortest (cut D) fragments after**
881 **re-amputation.** (A) DAPI-stained regenerates at 18 dpa. (B) Proglottid regeneration at 18 dpa.
882 N=3, n= 20 and 17; t-test, error bars = SD.
883

884 **Table S1. *βcatenin* paralogs.** BLASTp analysis indicates that *H. diminuta* has three *βcatenin*
885 paralogs with orthologs in other flatworms.
886
887 **Table S2. Primers and transcripts used in this study.**
888
889 **Table S3. All source data used in this study.**

Figure 1

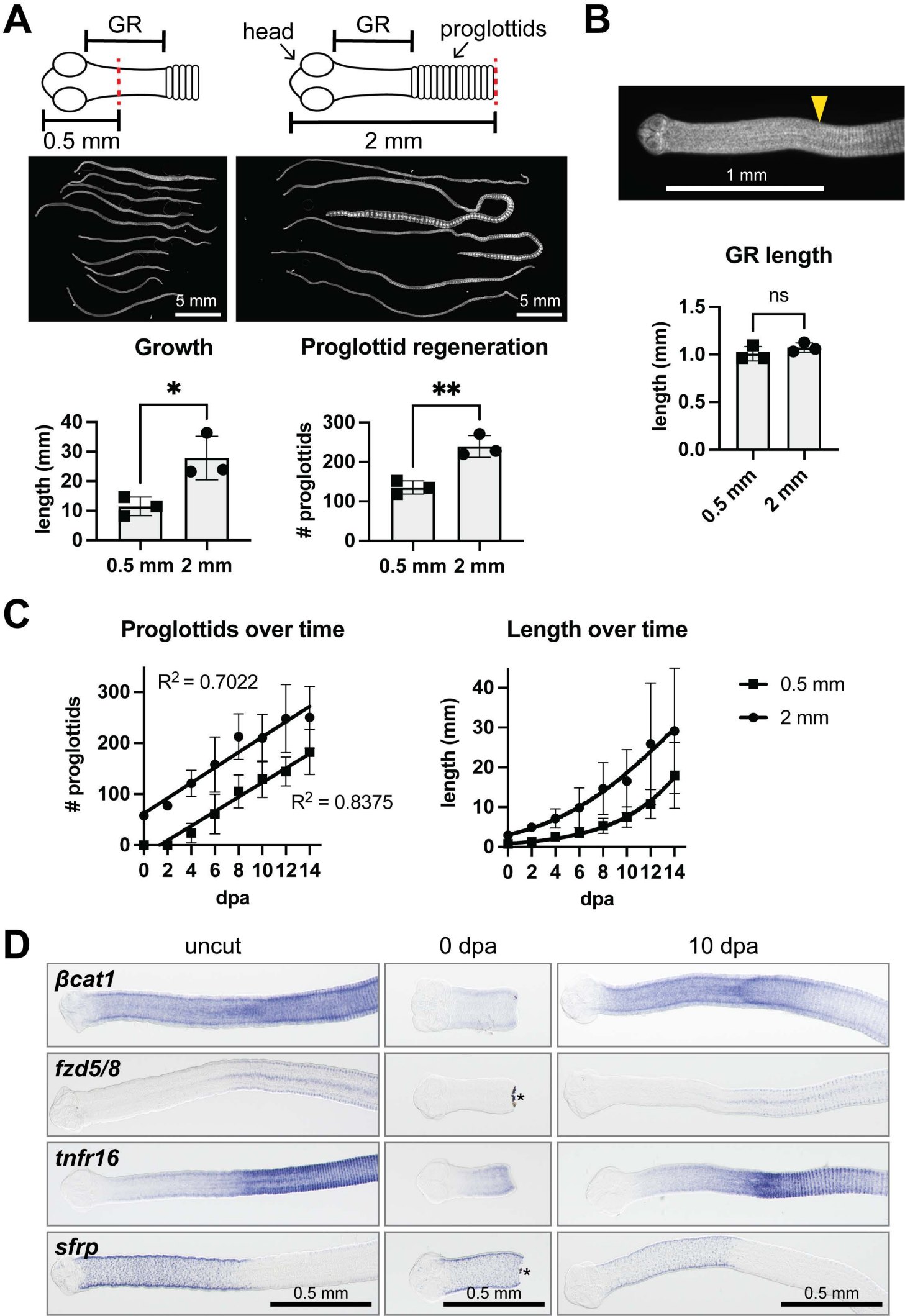
A
GR
0.5 mm
head
GR
proglottids
2 mm
5 mm
5 mm
Growth
Proglottid regeneration
*
**
length (mm)
proglottids
0.5 mm 2 mm
0.5 mm 2 mm
B
1 mm
GR length
ns
length (mm)
0.5 mm
2 mm
C
Proglottids over time
Length over time
R2 = 0.7022
R2 = 0.8375
# proglottids
length (mm)
dpa
dpa
0.5 mm
2 mm
D
uncut
0 dpa
10 dpa
βcat1
fzd5/8
tnfr16
sfrp
0.5 mm
0.5 mm
0.5 mm

Figure 2

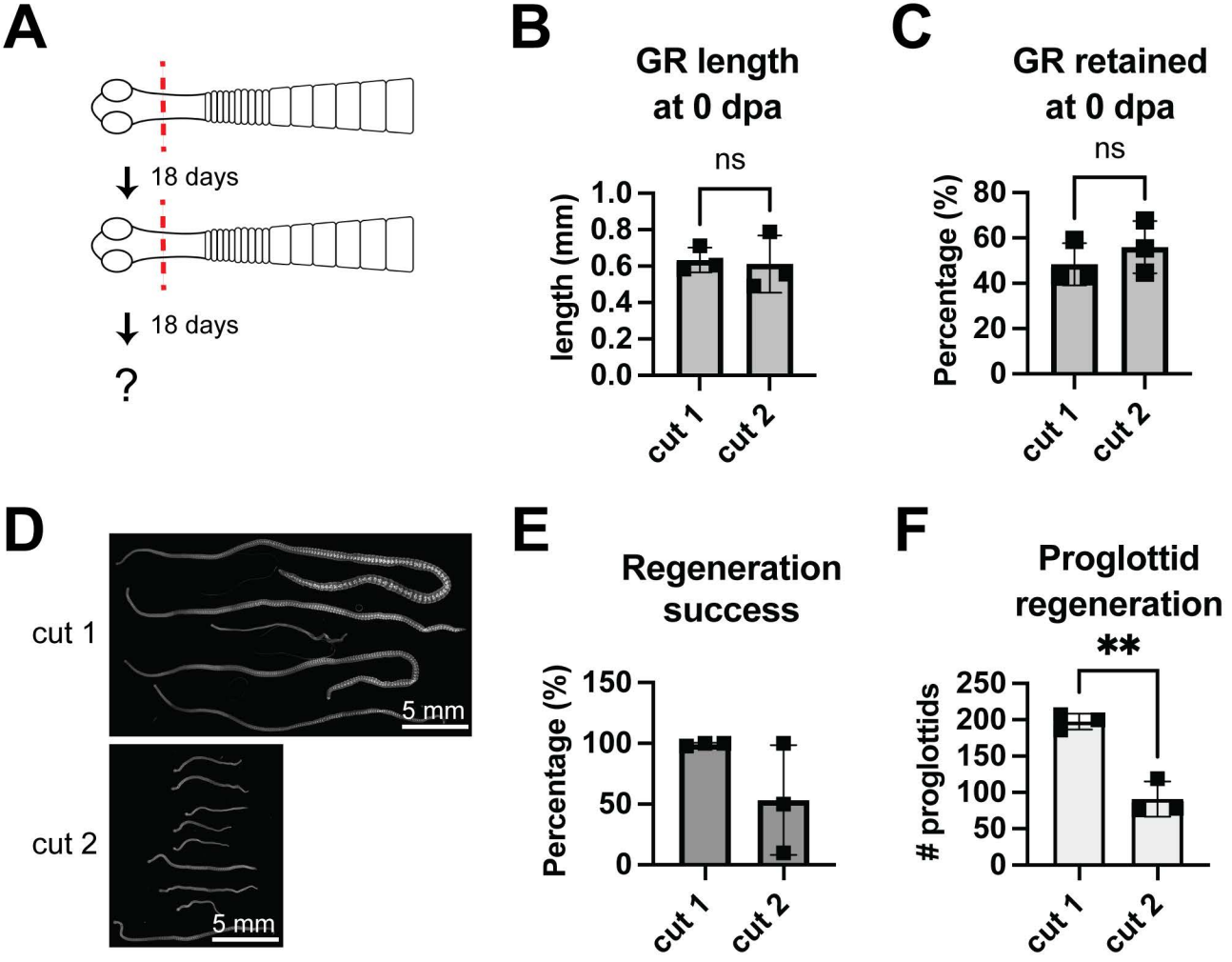
A
18 days
18 days
?
B
GR length at 0 dpa
ns
length (mm)
1.0
0.8
0.6
0.4
0.2
0.0
cut 1
cut 2
C
GR retained at 0 dpa
ns
Percentage (%)
80
60
40
20
0
cut 1
cut 2
D
cut 1
5 mm
cut 2
5 mm
E
Regeneration success
Percentage (%)
150
100
50
0
cut 1
cut 2
F
Proglottid regeneration
**
proglottids
250
200
150
100
50
0
cut 1
cut 2

Figure 3

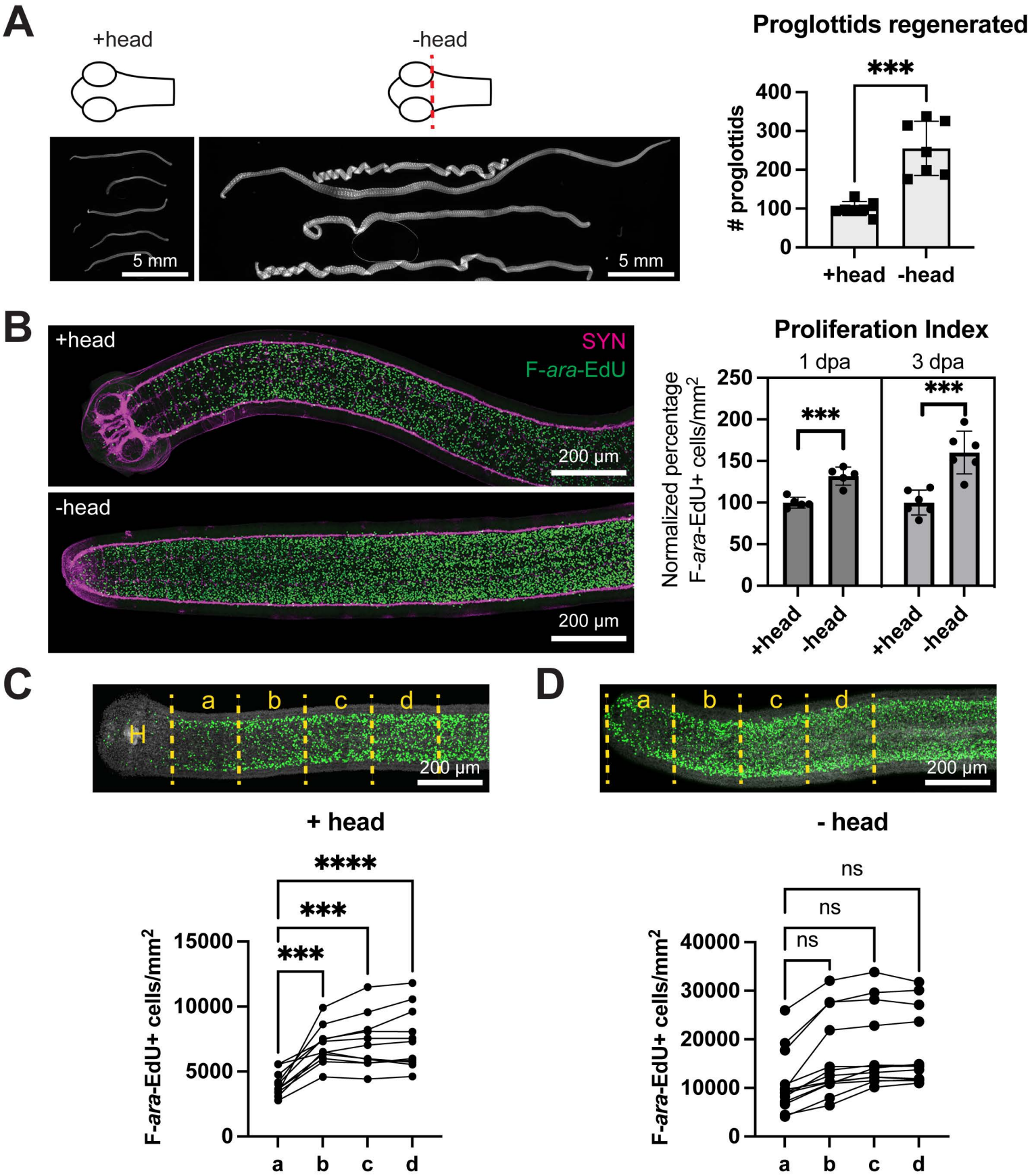
A
+head
-head
5 mm
5 mm
Proglottids regenerated
***
proglottids
400
300
200
100
0
+head
-head
B
+head
SYN
F-ara-EdU
200 µm
-head
200 µm
Proliferation Index
1 dpa
3 dpa
Normalized percentage F-ara-EdU+ cells/mm2
250
200
150
100
50
0
***
***
+head
-head
+head
-head
C
a
b
c
d
H
200 µm
+ head
****
***
***
F-ara-EdU+ cells/mm2
15000
10000
5000
0
a
b
c
d
D
a
b
c
d
200 µm
- head
ns
ns
ns
F-ara-EdU+ cells/mm2
40000
30000
20000
10000
0
a
b
c
d

Figure 4

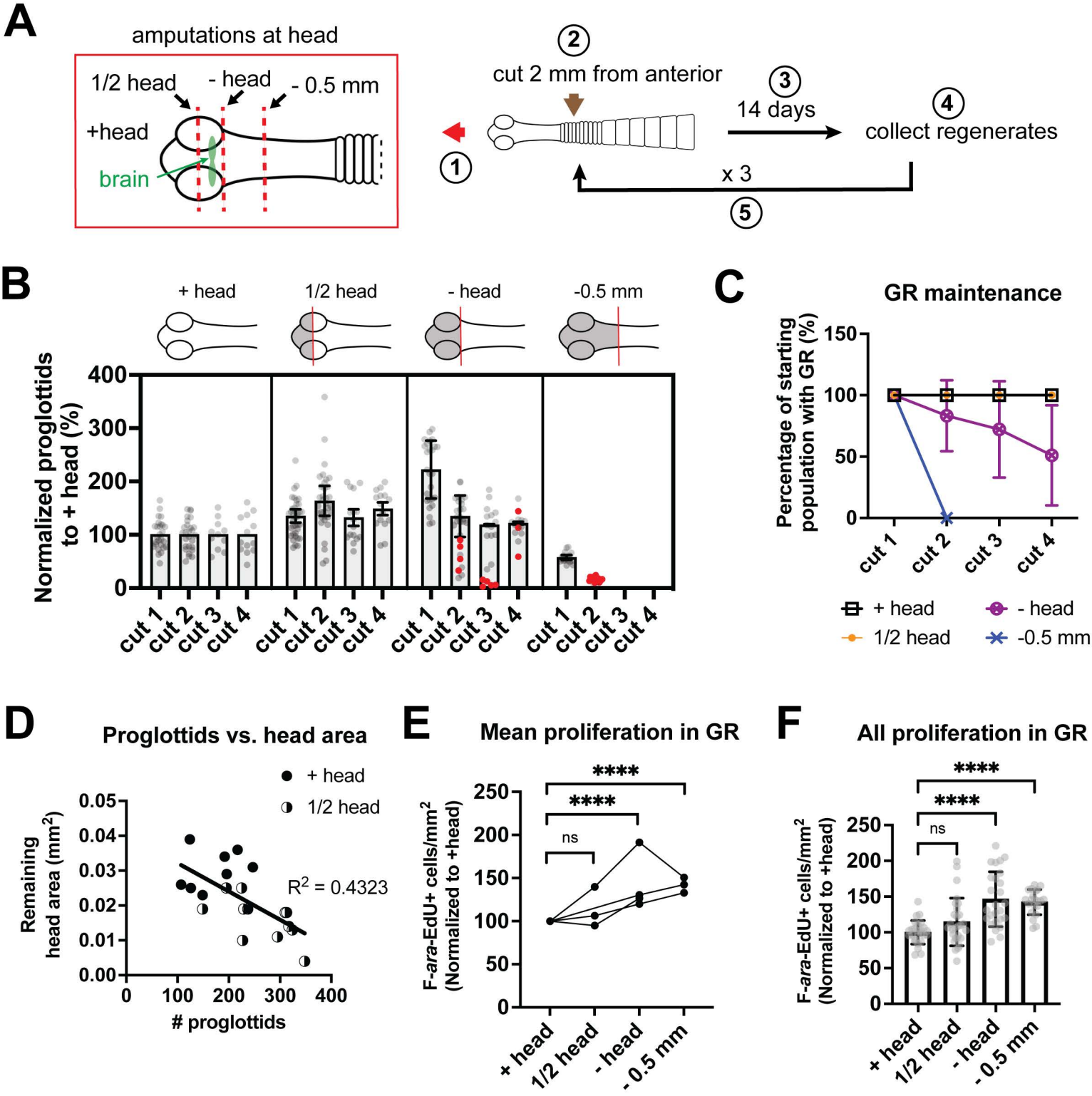
A
amputations at head
1/2 head
- head
- 0.5 mm
+head
brain
1
2
cut 2 mm from anterior
3
14 days
4
collect regenerates
x 3
5
B
+ head
1/2 head
- head
-0.5 mm
Normalized proglottids to + head (%)
400
300
200
100
0
cut 1
cut 2
cut 3
cut 4
C
GR maintenance
Percentage of starting population with GR (%)
150
100
50
0
cut 1
cut 2
cut 3
cut 4
+ head
- head
1/2 head
-0.5 mm
D
Proglottids vs. head area
+ head
1/2 head
Remaining head area (mm²)
0.05
0.04
0.03
0.02
0.01
0.00
R² = 0.4323
0
100
200
300
400
proglottids
E
Mean proliferation in GR
F-ara-EdU+ cells/mm² (Normalized to +head)
250
200
150
100
50
0
****
****
ns
+ head
1/2 head
- head
- 0.5 mm
F
All proliferation in GR
F-ara-EdU+ cells/mm² (Normalized to +head)
250
200
150
100
50
0
****
****
ns
+ head
1/2 head
- head
- 0.5 mm

Figure 5

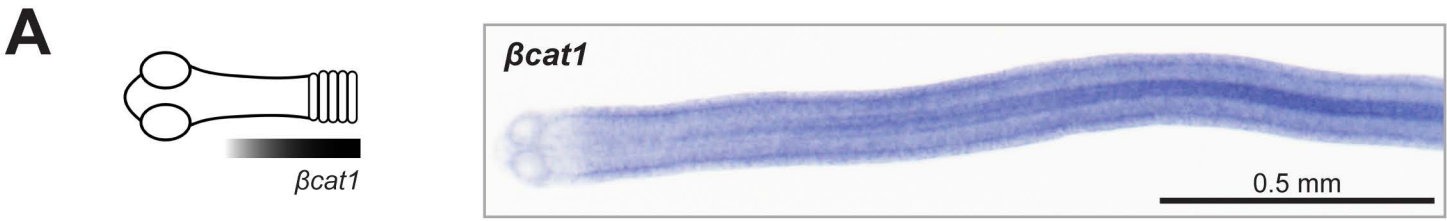
A
βcat1
βcat1
0.5 mm

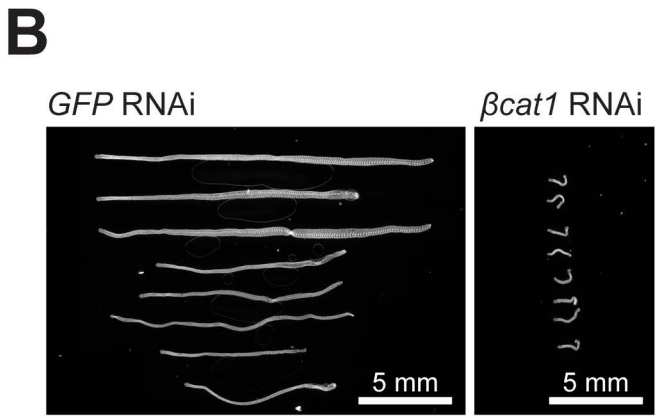
B
GFP RNAi
βcat1 RNAi
5 mm
5 mm

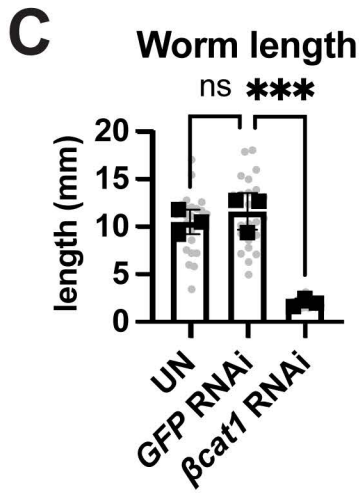
C
Worm length
ns
***
length (mm)
20
15
10
5
0
UN
GFP RNAi
βcat1 RNAi

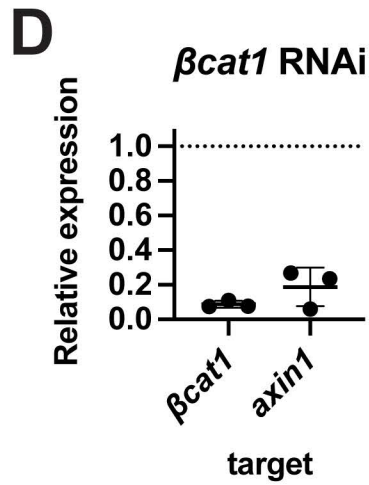
D
βcat1 RNAi
Relative expression
1.0
0.8
0.6
0.4
0.2
0.0
βcat1
axin1
target

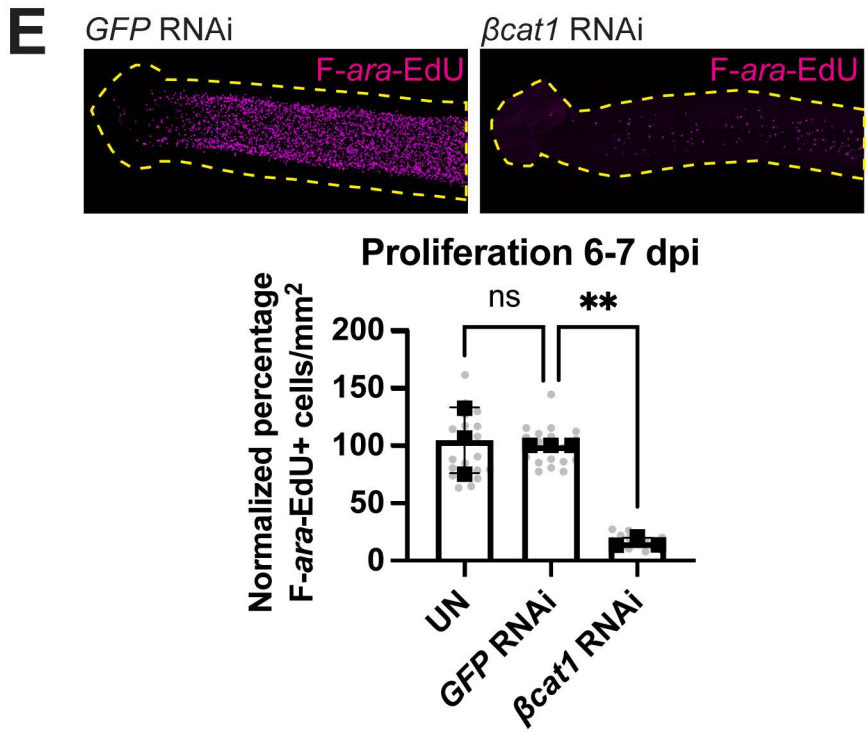
E
GFP RNAi
βcat1 RNAi
F-ara-EdU
F-ara-EdU
Proliferation 6-7 dpi
ns
**
Normalized percentage
F-ara-EdU+ cells/mm2
200
150
100
50
0
UN
GFP RNAi
βcat1 RNAi

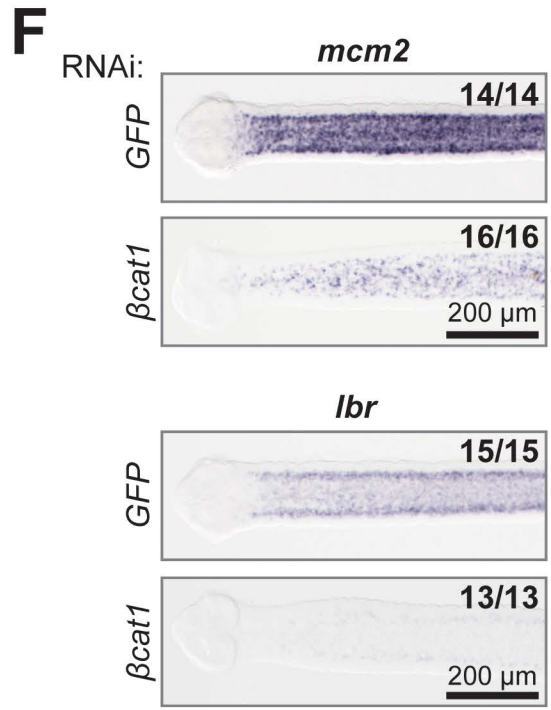
F
RNAi:
mcm2
GFP
14/14
βcat1
16/16
200 µm
lbr
GFP
15/15
βcat1
13/13
200 µm

Figure 6

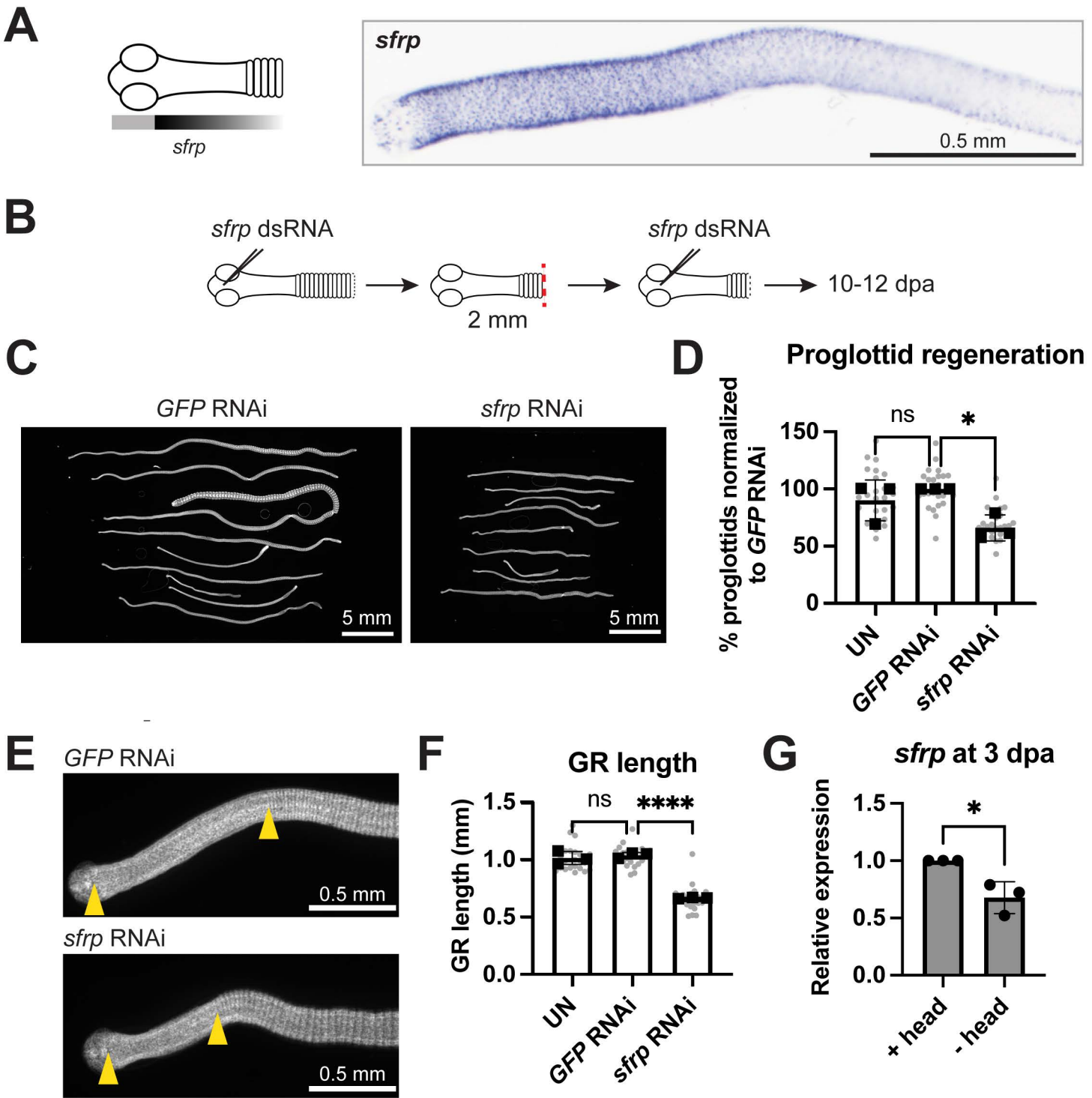
A
sfrp
sfrp
0.5 mm
B
sfrp dsRNA
2 mm
sfrp dsRNA
10-12 dpa
C
GFP RNAi
sfrp RNAi
5 mm
5 mm
D
Proglottid regeneration
% proglottids normalized to GFP RNAi
150
100
50
0
ns
*
UN
GFP RNAi
sfrp RNAi
E
GFP RNAi
0.5 mm
sfrp RNAi
0.5 mm
F
GR length
GR length (mm)
1.5
1.0
0.5
0.0
ns
****
UN
GFP RNAi
sfrp RNAi
G
sfrp at 3 dpa
Relative expression
1.5
1.0
0.5
0.0
*
+ head
- head

Figure 7

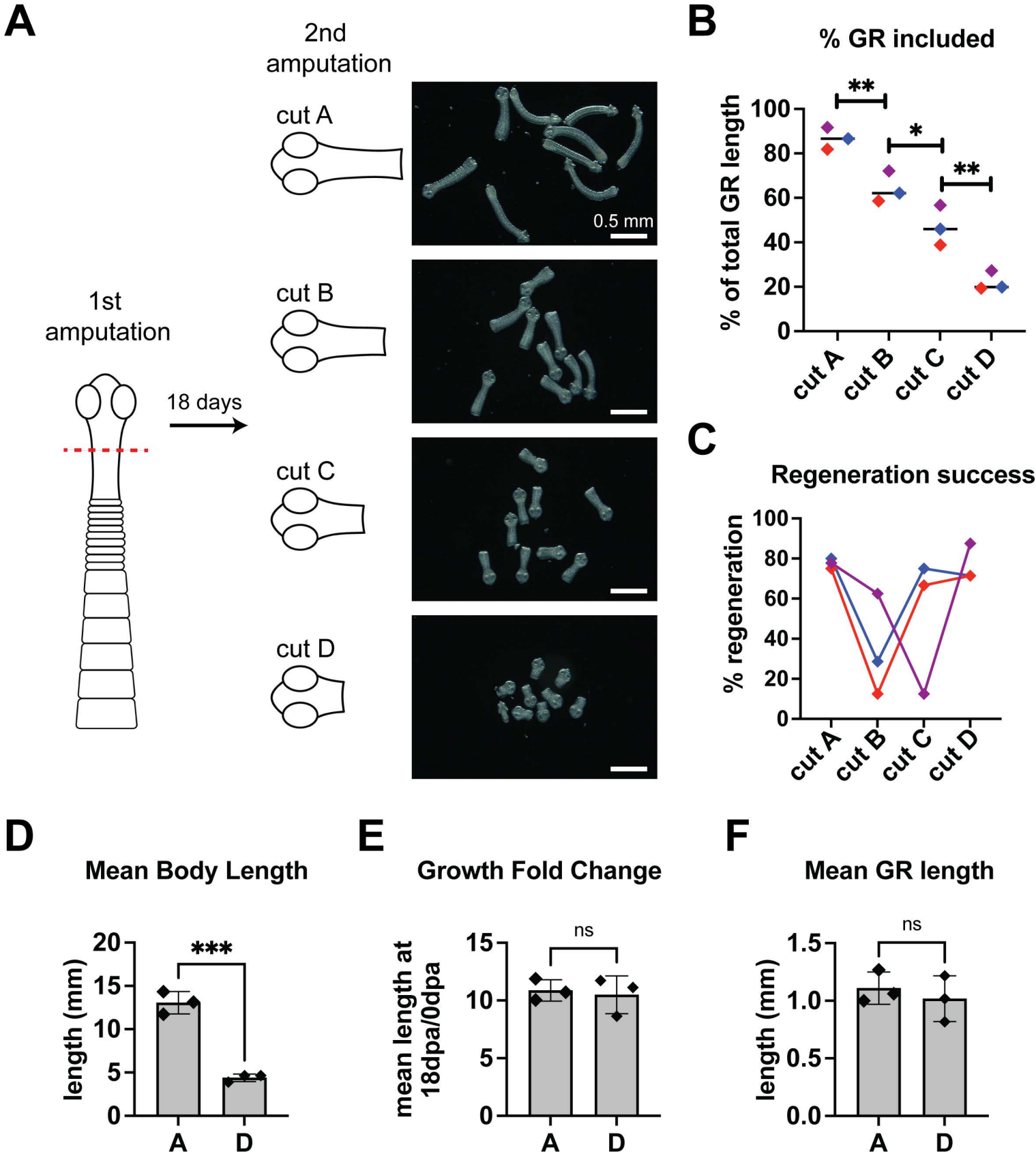
A
2nd amputation
cut A
cut B
cut C
cut D
1st amputation
18 days
0.5 mm
B
% GR included
% of total GR length
100
80
60
40
20
0
**
*
**
cut A
cut B
cut C
cut D
C
Regeneration success
% regeneration
100
80
60
40
20
0
cut A
cut B
cut C
cut D
D
Mean Body Length
length (mm)
20
15
10
5
0
***
A
D
E
Growth Fold Change
mean length at 18dpa/0dpa
15
10
5
0
ns
A
D
F
Mean GR length
length (mm)
1.5
1.0
0.5
0.0
ns
A
D

Figure 8

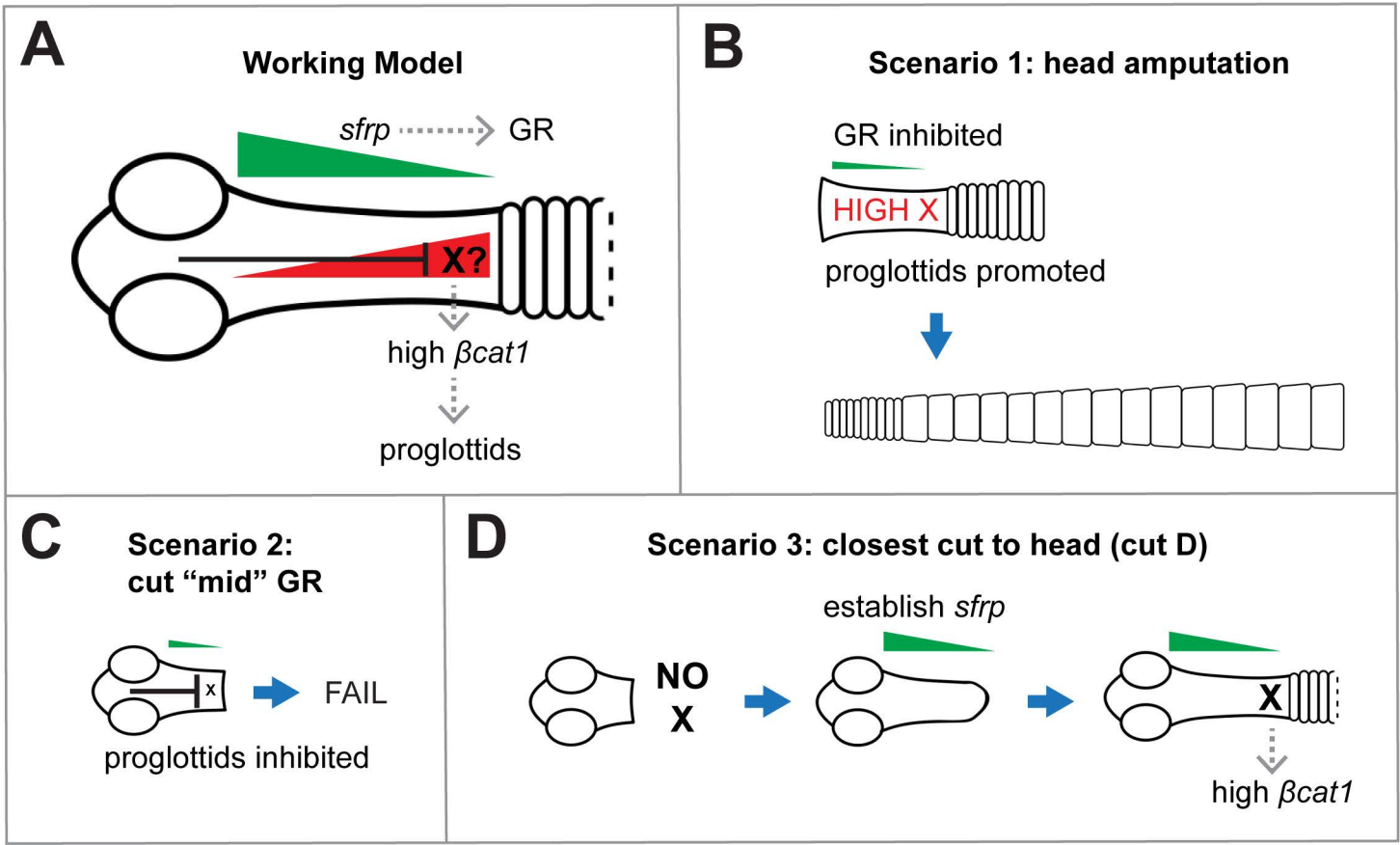
A
Working Model
sfrp
GR
X?
high βcat1
proglottids
B
Scenario 1: head amputation
GR inhibited
HIGH X
proglottids promoted
C
Scenario 2:
cut "mid" GR
x
FAIL
proglottids inhibited
D
Scenario 3: closest cut to head (cut D)
establish sfrp
NO
X
X
high βcat1

Figure S1

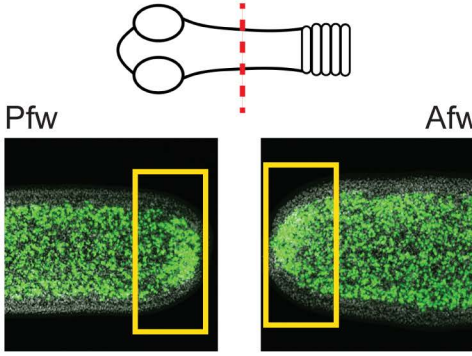
Pfw
Afw

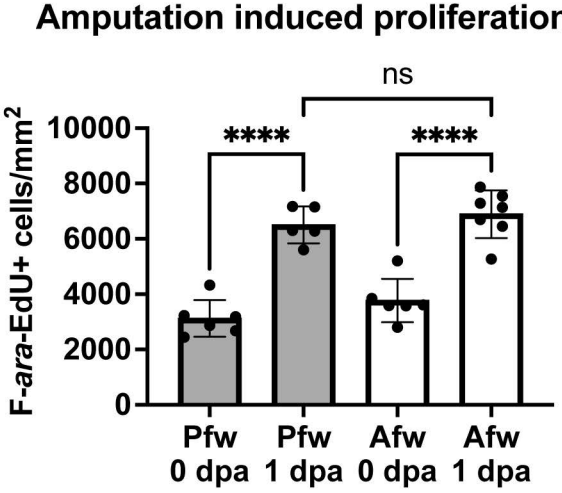
Amputation induced proliferation
ns
****
****
F-ara-EdU+ cells/mm2
10000
8000
6000
4000
2000
0
Pfw 0 dpa
Pfw 1 dpa
Afw 0 dpa
Afw 1 dpa

Figure S2

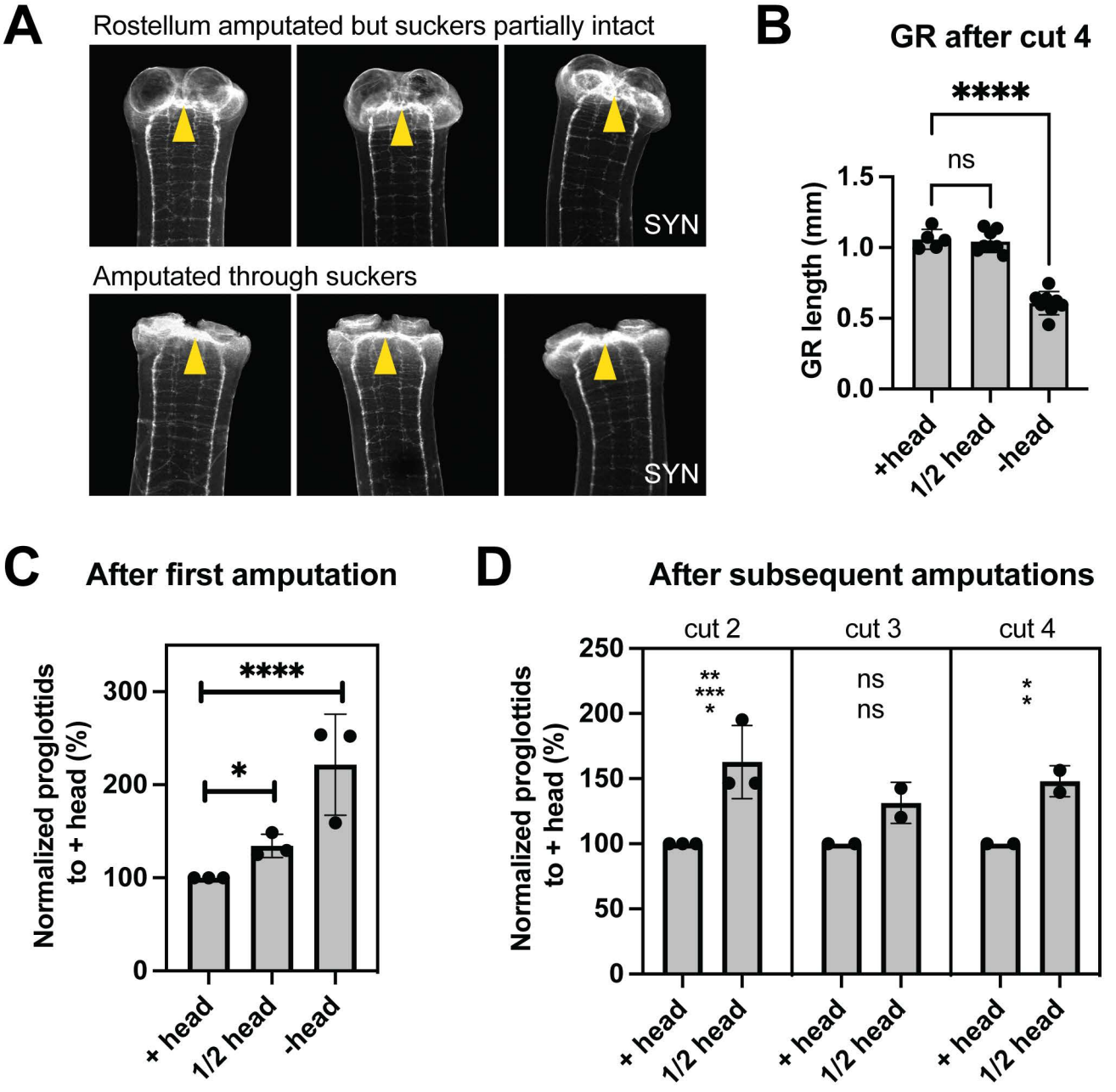
A
Rostellum amputated but suckers partially intact
SYN
Amputated through suckers
SYN
B
GR after cut 4
****
ns
GR length (mm)
1.5
1.0
0.5
0.0
+head
1/2 head
-head
C
After first amputation
****
*
Normalized proglottids to + head (%)
300
200
100
0
+ head
1/2 head
-head
D
After subsequent amputations
cut 2
cut 3
cut 4
**
***
*
ns
ns
*
*
Normalized proglottids to + head (%)
250
200
150
100
50
0
+ head
1/2 head
+ head
1/2 head
+ head
1/2 head

Figure S3

A

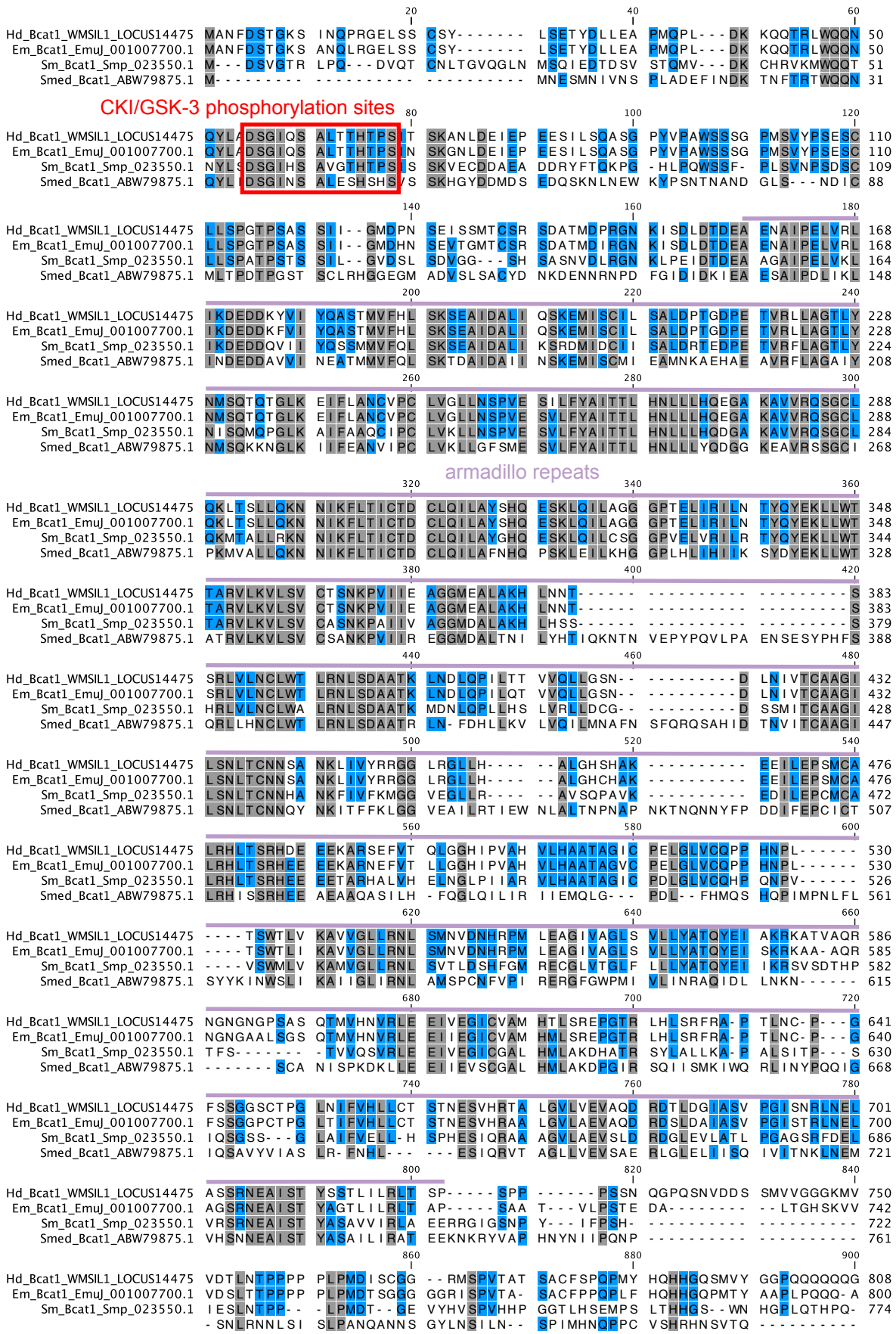
CKI/GSK-3 phosphorylation sites
armadillo repeats
Hd_Bcat1_WMSIL1_LOCUS14475
Em_Bcat1_EmuJ_001007700.1
Sm_Bcat1_Smp_023550.1
Smed_Bcat1_ABW79875.1

```
                                                  920                                 940                                 960
                                                   |                                   |                                   |
Hd_Bcat1_WMSIL1_LOCUS14475  PPLQRYAPPP  PGSYHYSNNE  PVGSGGNGGG  ----SLMAMV  GPPPNSSAYS  GGNS-----G  859
 Em_Bcat1_EmuJ_001007700.1  PSVQRYAP--  -GGYHYSGEA  VAGPGGGGGG  GSGGSLMAMV  GPPPPASVYS  VSGS-----G  852
     Sm_Bcat1_Smp_023550.1  ----------  ----------  ---ESGNTCG  SPSNSLMEML  GPFPPGCKGS  VCNDCCSYWG  811
     Smed_Bcat1_ABW79875.1  ----------  ----------  --------CG  DQNIATNETL  ----------  ----------  820
                                                  980                                1,000                               1,020
                                                   |                                   |                                   |
Hd_Bcat1_WMSIL1_LOCUS14475  GCPMNVQQQM  PPQQ-HPPHC  YQQQPMNENA  YQQCSWGNPS  YPQEPQGRPV  YANQMPPHHA  918
 Em_Bcat1_EmuJ_001007700.1  PCPMSVQS-M  PPQQ-HP-HC  YQQQPMNEAA  YPQRSWGNGP  YASDPQGRPL  YANTMAPHHP  909
     Sm_Bcat1_Smp_023550.1  DCD-------  PPGTCSDPNC  IYNG------  --NNSQSSGT  Y-SELQPVKL  YHNI------  849
     Smed_Bcat1_ABW79875.1  -CPIN---DV  DVTDYHMPFS  NTLQPQNR--  ----------  YPYNP-----  --NFVDPNYS  857
                                                 1,040                               1,060                               1,080
                                                   |                                   |                                   |
Hd_Bcat1_WMSIL1_LOCUS14475  PPAQQPQSQE  GMYGPPGMGY  IQP---SGNM  RGVQPAYHHR  SSPAAAQGGY  Y---------  966
 Em_Bcat1_EmuJ_001007700.1  PPAQQ--QQE  TLYGPPGMGY  PPP---SGSV  RDMPPAYHHR  GSPAAA--GY  Y---------  953
     Sm_Bcat1_Smp_023550.1  ----RSSSRT  GFVGCGNTYS  VGPTFVSSSV  QNIDNTHQLQ  GSNPVLPNGM  SVVPRRSCVG  905
     Smed_Bcat1_ABW79875.1  LINQTGNSEI  AMRHFKQMGS  INISNECVN-  QDVQKAY---  ----------  ----------  893
                                                 1,100                               1,120                               1,140
                                                   |                                   |                                   |
Hd_Bcat1_WMSIL1_LOCUS14475  ---GGGYMDT  QQGPPPQGGP  M-TSPNPRGC  YSTTAP----  ---SSMDTT-  NSTNGYASPG  1014
 Em_Bcat1_EmuJ_001007700.1  ---AGGYIEP  QQ-PPPQAGP  M-TSPNPRAC  YPTNTP----  ---SSMDTT-  TSTSGYTSPG  1000
     Sm_Bcat1_Smp_023550.1  SISSSGYLSP  -------GGD  MFLNPSPSEY  KPFHEDNQGI  LRSSLLDQQ-  THTASISSPA  957
     Smed_Bcat1_ABW79875.1  --SNSSFKSP  SSHSLSVSGN  L--------C  SSNENSKKDM  MDVCMLDADW  IETCSDFSQG  943
                                                 1,160                               1,180
                                                   |                                   |
Hd_Bcat1_WMSIL1_LOCUS14475  TASRMAMGDD  YMT--PVMET  TMKPSVNPST  PNSTSSSGNQ  PDHRWFSSAQ  MCLP  1066
 Em_Bcat1_EmuJ_001007700.1  TAGRMALGDD  FMTGTPVLDG  GVKPSANPST  P---TSSGAP  PDHRWFSSAQ  MCLP  1051
     Sm_Bcat1_Smp_023550.1  IPSRNV----  ----------  ----NAGYLS  PDLMALEETD  PD--WFGGPA  VM--  989
     Smed_Bcat1_ABW79875.1  HSQKS-----  ----------  ----------  ----------  ----W----S  PINK  954
```

B

```
                                  α  α   α          α    α   α  α  α   α
Human_CTNB1_sp|P35222.1|  TNVQRLAEPS  QMLKHAVVNL  INYQDD

Smed_Bcat2_ABW79874.1  SSMIRMQKPA  QRLRFLVTNM  IDYIED
Em_Bcat2_EmuJ_001103600.1  FAVQRLSPCI  ESLTKAIGMI  INFKDD
Hd_Bcat2_WMSIL1_LOCUS880.1  SAVLRLSPCI  SNLAKAIGMV  INFKD

Smed_Bcat1_ABW79875.1  ADVSLSACYD  NKDENNRNPD  FGIDID
Em_Bcat1_EmuJ_001007700.1  SEVTGMTCSR  SDATMDIRGN  KISDLD
Hd_Bcat1_WMSIL1_LOCUS14475  SEISSMTCSR  SDATMDPRGN  KISDLD
```

Figure S4

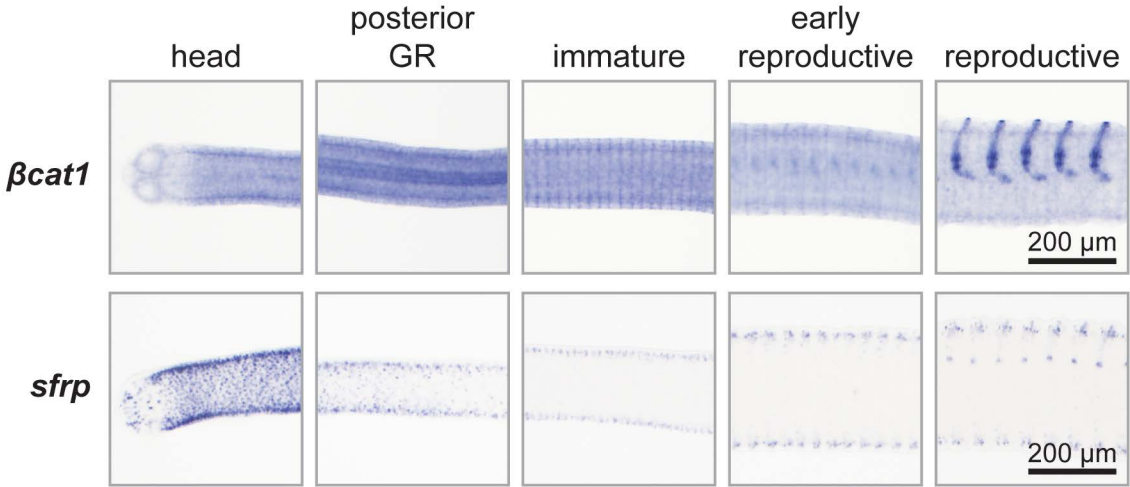
head
posterior GR
immature
early reproductive
reproductive
βcat1
sfrp
200 µm
200 µm

Figure S5

```
                                         20                          40                          60
                                          |                           |                           |
Hd_sfrp_HD_tophat_13573  M---------  ----LYLLLL  IFIAITSRGN  TVGRWDWNR-  ---VNKTSVT  TAPFGGGAFG  43
Em_sfrp_EmuJ_000838700.1 M---------  ----LPLVIL  FAIS-AAQAN  TVGRWDWHRG  GGAKNKTAVT  SSPFGGTSLS  46
Smed_sfrp1_ABY85212.1    MEMTKI----  ----FPLSLL  LFISNV----  ----------  ----------  ----------  18
Human_SFRP1_sp|Q8N474.1| MGIGRSEGGR  RGAALGVLLA  LGAALLAVGS  ----------  ----------  ----------  30
Human_SFRP5_sp|Q5T4F7.3| MRAAAAGGGV  RTAALALLL-  -GALHWAPAR  ----------  ----------  ----------  28
Human_SFRP2_sp|Q96HF1.2| MLQGPG----  -----SLLLL  FLASHCCLGS  ----------  ----------  ----------  21

                                         80                         100                         120
                                          |                           |                           |
Hd_sfrp_HD_tophat_13573  RLTTADADMI  SNEPPQSPYF  SDWNRLVSG-  -YGSQ-RCYK  IPKELKLCHK  IGYDLMVLPN  100
Em_sfrp_EmuJ_000838700.1 RLTTADVHMI  SNEPPQSPYF  SDWNRLVSG-  -YGSQ-RCYK  IPRGMKLCHK  IGYDFMVLPN  103
Smed_sfrp1_ABY85212.1    ----------  ------NSFI  GDWQAFQSG-  -YTID-QCYQ  IPDNFTLCSN  VGYRLMVLPN  59
Human_SFRP1_sp|Q8N474.1| ----------  ASEYDYVSFQ  SDIGPYQSGR  FYTKPPQCVD  IPADLRLCHN  VGYKKMVLPN  80
Human_SFRP5_sp|Q5T4F7.3| ----------  CEEYDYYGWQ  AE--PLH-GR  SYSKPPQCLD  IPADLPLCHT  VGYKRMRLPN  75
Human_SFRP2_sp|Q96HF1.2| ----------  ARGLFLFG-Q  PDF-------  SY-KRSNCKP  IPANLQLCHG  IEYQNMRLPN  62
```

Frizzled domain

```
                                        140                         160                         180
                                          |                           |                           |
Hd_sfrp_HD_tophat_13573  SLEHEGMDEV  ITQSEVWLTL  VNLGCHDELE  RFLCSLYAPV  CIRGYHEKLI  QPCRELCESV  160
Em_sfrp_EmuJ_000838700.1 SLEHETLDEA  ITQSEVWLTL  VNLGCHDELK  RFLCSLYAPV  CINGYHEKLI  QPCRELCESV  163
Smed_sfrp1_ABY85212.1    YIQHESIEEA  AQHSKVWMGL  VNTQCHVDIK  KFICSLYAPV  CISNQRNQKV  PPCRELCVTV  119
Human_SFRP1_sp|Q8N474.1| LLEHETMAEV  KQQASSWVPL  LNKNCHAGTQ  VFLCSLFAPV  CLD----RPI  YPCRWLCEAV  136
Human_SFRP5_sp|Q5T4F7.3| LLEHESLAEV  KQQASSWLPL  LAKRCHSDTQ  VFLCSLFAPV  CLD----RPI  YPCRSLCEAV  131
Human_SFRP2_sp|Q96HF1.2| LLGHETMKEV  LEQAGAWIPL  VMKQCHPDTK  KFLCSLFAPV  CLDDL-DETI  QPCHSLCVQV  121

                                        200                         220                         240
                                          |                           |                           |
Hd_sfrp_HD_tophat_13573  RAACLPTMTT  FGLGWPDIVK  CSKFPQAPQE  LCIPPNKQRN  KTVVLKPETR  -CSGCVDKPT  219
Em_sfrp_EmuJ_000838700.1 RAACLPTMTT  FGLGWPDIVK  CSKFPQAPQE  LCIPLNKHKN  KTIILNPETR  -CSGCIDRPT  222
Smed_sfrp1_ABY85212.1    KESCLPSMKM  YGFDWPTIMK  CSKFPQFKNS  LCIP------  K-VV--PGKK  -CDLCMKIAS  170
Human_SFRP1_sp|Q8N474.1| RDSCEPVMQF  FGFYWPEMLK  CDKFP--EGD  VCIAMTPPNA  TEASKPQGTT  VCPPCDNELK  194
Human_SFRP5_sp|Q5T4F7.3| RAGCAPLMEA  YGFPWPEMLH  CHKFPL-DND  LCIAVQFGHL  P-ATAPPVTK  ICAQCEMEHS  189
Human_SFRP2_sp|Q96HF1.2| KDRCAPVMSA  FGFPWPDMLE  CDRFPQ-DND  LCIPLASSDH  LLPATEEAPK  VCEACKNKND  180
```

Netrin domain

```
                                        260                         280                         300
                                          |                           |                           |
Hd_sfrp_HD_tophat_13573  YES-AIGSFC  TADVAVRSKV  LDLIPVPSTK  GQNTTYRIRT  DGRGGIFKM-  ---PKNVNKE  274
Em_sfrp_EmuJ_000838700.1 YES-AIGSFC  TADVVIRAKV  LDLVPTLPSS  GHNTTHRIRT  TGRVGAFKL-  ---PKTLNSI  277
Smed_sfrp1_ABY85212.1    YEV-IANRFC  LSPIVIRAKI  KRIIP---TS  GN--AIQIIL  QKKSKFLKF-  ---QANFSQN  220
Human_SFRP1_sp|Q8N474.1| SEA-IIEHLC  ASEFALRMKI  KEV-----KK  ENGDKKIV--  PKKKKPLKLG  PIKKKDLKKL  246
Human_SFRP5_sp|Q5T4F7.3| ADG-LMEQMC  SSDFVVKMRI  KEI-----KI  ENGDRKLIGA  QKKKKLLKPG  PLKRKDTKRL  243
Human_SFRP2_sp|Q96HF1.2| DDNDIMETLC  KNDFALKIKV  KEI-----TY  INRDTKIILE  TKSKTIYKLN  GVSERDLKKS  235

                                        320                         340                         360
                                          |                           |                           |
Hd_sfrp_HD_tophat_13573  A-NLDFRMTC  DCPIIKAAMT  RSKGPGRWLL  MGKLNEDGRS  VTVLHLSQPS  RQNKGIKRAI  333
Em_sfrp_EmuJ_000838700.1 V-NLEFEMEC  DCPIIRAALT  RQKGPGRWLM  MGKLNDDRRT  VTVQHISQPS  RQNAGIKRAI  336
Smed_sfrp1_ABY85212.1    A--LELNLKC  NCTNLKFKQR  ALKG--RWII  MAQIDSDNKA  V-VNFISKWK  RKKAEFKHSM  275
Human_SFRP1_sp|Q8N474.1| VLYLKNGADC  PCHQLDNLS-  -----HHFLI  MGR--KVKSQ  YLLTAIHKWD  KKNKEFKNFM  298
Human_SFRP5_sp|Q5T4F7.3| VLHMKNGAGC  PCPQLDSLA-  -----GSFLV  MGR--KVDGQ  LLLMAVYRWD  KKNKEMKFAV  295
Human_SFRP2_sp|Q96HF1.2| VLWLKDSLQC  TCEEMNDIN-  -----APYLV  MGQ--KQGGE  LVITSVKRWQ  KGQREFKRIS  287

                                        380                         400                         420
                                          |                           |                           |
Hd_sfrp_HD_tophat_13573  KEMRHQPDTL  CKVDLTRSSP  VVHPRTVAGR  PAANGAQISQ  EQKQQHQQLQ  PRRNGSNLSK  393
Em_sfrp_EmuJ_000838700.1 RDIRRRPDSL  CKVDLMHPNP  VAHSRAISSL  SSPSSMQSLR  PRSHQSRRYR  P-----HLSP  391
Smed_sfrp1_ABY85212.1    KIIQNFGHIV  CKSKLPDGIS  L-RERYAAYL  KMNNQLKYSN  ERKLQTRKFR  ---------K  325
Human_SFRP1_sp|Q8N474.1| KKMKNHE---  CPTFQSVF--  ----K-----  ----------  ----------  ----------  314
Human_SFRP5_sp|Q5T4F7.3| KFMFSYP---  CSLYYPFFYG  AAEPH-----  ----------  ----------  ----------  317
Human_SFRP2_sp|Q96HF1.2| RSIRKLQ---  C---------  ----------  ----------  ----------  ----------  295

                                        440                         460                         480
                                          |                           |                           |
Hd_sfrp_HD_tophat_13573  EERRRRRQLR  RRRNE---AG  AQQQQHPSNV  TLSSTNSQES  QQPVNDMPIG  VNTQHPYNQQ  450
Em_sfrp_EmuJ_000838700.1 EERRRR-QLR  RRRNHPRGSS  PEAQQRAANV  TPSRKPPQLQ  QQPINDIPIL  TPTPRPFSHH  450
Smed_sfrp1_ABY85212.1    QKSRK-----  ---------S  VKPNNRSAGI  S---------  ----------  ----------  342
Human_SFRP1_sp|Q8N474.1| ----------  ----------  ----------  ----------  ----------  ----------  314
Human_SFRP5_sp|Q5T4F7.3| ----------  ----------  ----------  ----------  ----------  ----------  317
Human_SFRP2_sp|Q96HF1.2| ----------  ----------  ----------  ----------  ----------  ----------  295
```

Figure S6

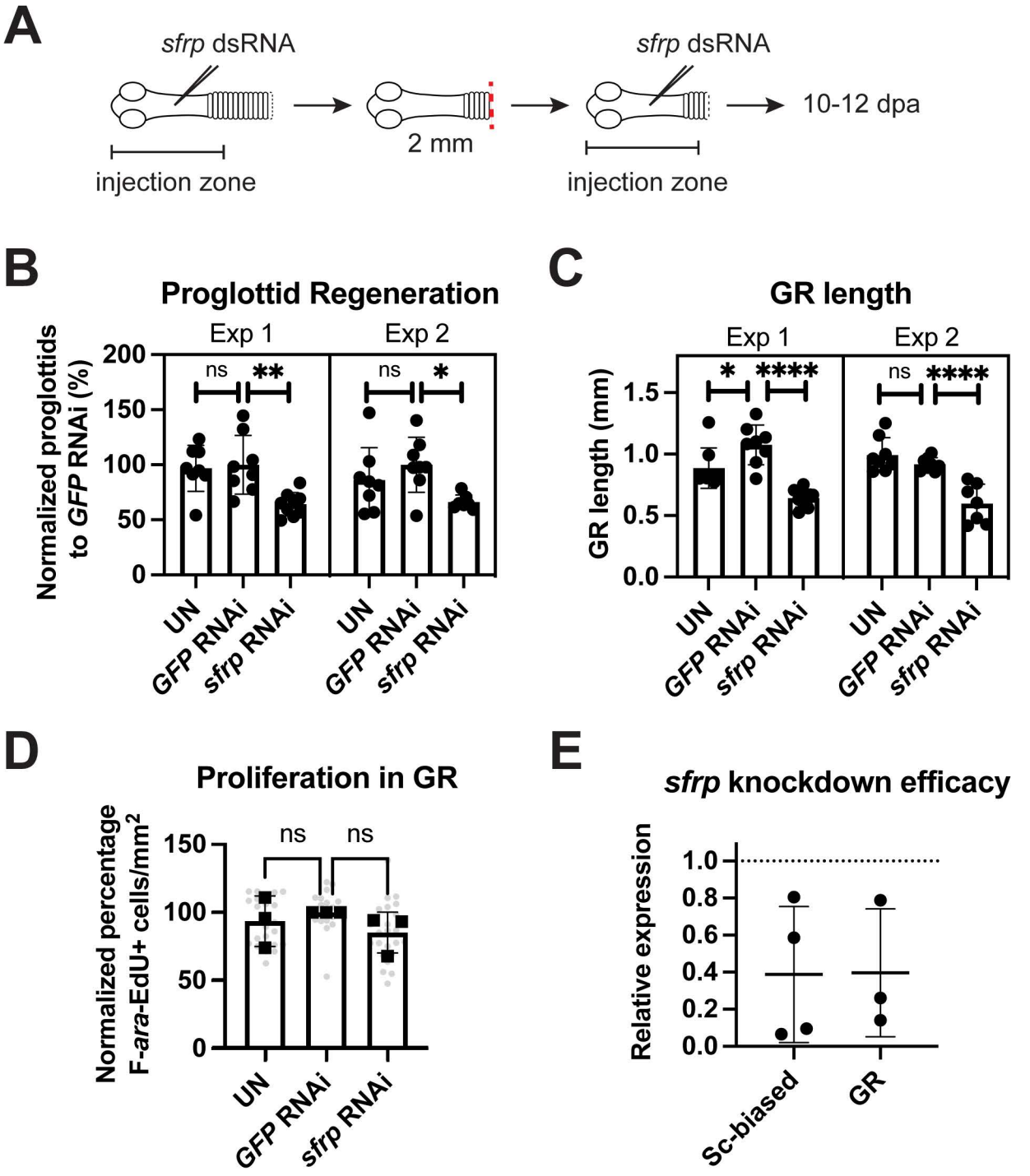
A
sfrp dsRNA
sfrp dsRNA
10-12 dpa
2 mm
injection zone
injection zone
B
Proglottid Regeneration
Exp 1
Exp 2
Normalized proglottids to GFP RNAi (%)
200
150
100
50
0
ns
**
ns
*
UN
GFP RNAi
sfrp RNAi
C
GR length
Exp 1
Exp 2
GR length (mm)
1.5
1.0
0.5
0.0
*
****
ns
****
UN
GFP RNAi
sfrp RNAi
D
Proliferation in GR
Normalized percentage F-ara-EdU+ cells/mm2
150
100
50
0
ns
ns
UN
GFP RNAi
sfrp RNAi
E
sfrp knockdown efficacy
Relative expression
1.0
0.8
0.6
0.4
0.2
0.0
Sc-biased
GR

Figure S7

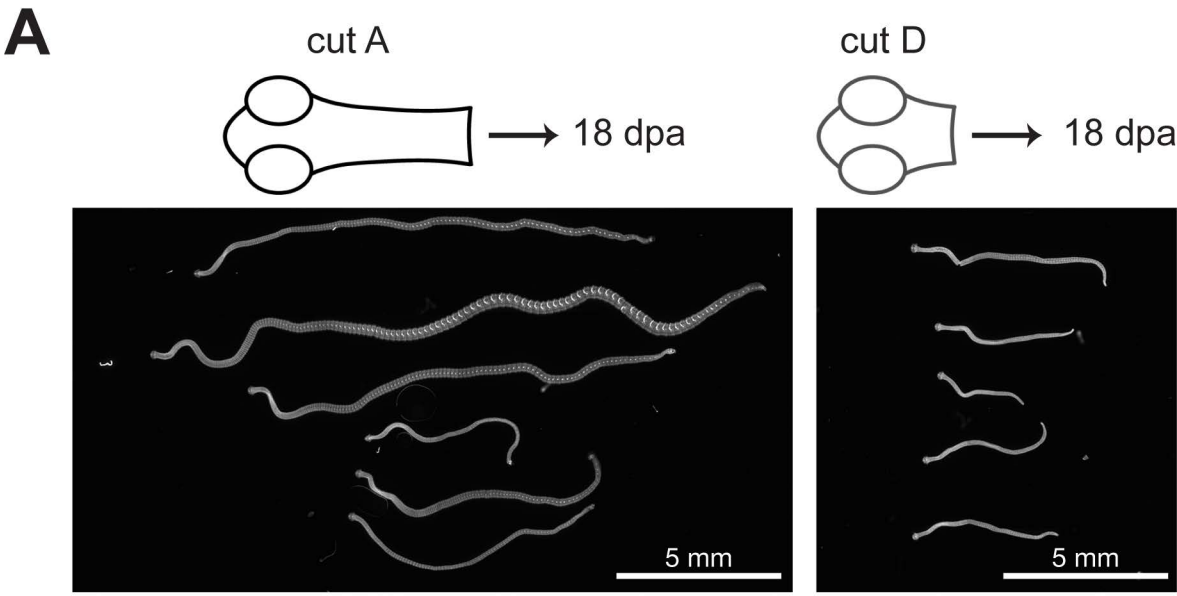
A
cut A
18 dpa
cut D
18 dpa
5 mm
5 mm

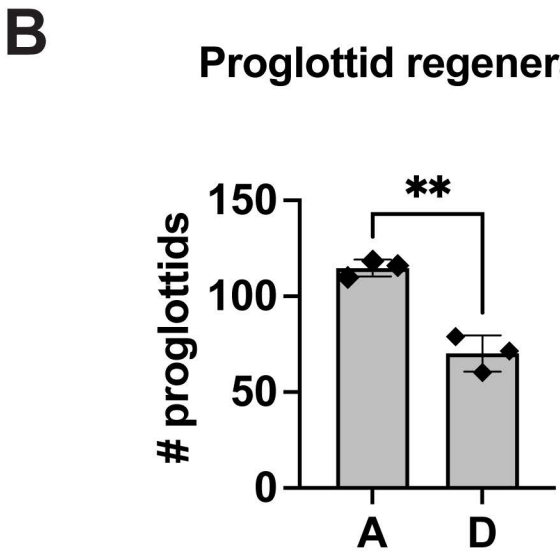
B
Proglottid regeneration
proglottids
150
100
50
0
**
A
D